# Integration of Health Monitoring and Control of Building Structures due to Earthquake with Test Validation

Henry T Y Yang, M. ASCE [1], Jiazeng Shan [2], Connor J. Randall [3], Paul K Hansma [4] and Weixing Shi [5]

**Abstract**

A hybrid real-time structural health monitoring and control system for building structures is presented in this study. A model-reference adaptive control algorithm for the decoupled substructures was developed and integrated with a previously developed interstory drift based acceleration feedback method for health monitoring. Little or no prior information about current health condition of the structure is required by the proposed adaptive control algorithm. A virtual healthy model, installed with health monitors, is utilized to generate proper control forces to obtain the desired response for the controlled substructure during a disastrous event such as an earthquake. An adaptive controller and an adaptation mechanism are designed using the Lyapunov theory to calculate the real-time adaptive control force. The local feedback control actuates the

[1] Professor, Department of Mechanical Engineering, University of California, Santa Barbara, CA 93106, USA

[2] PhD Candidate, Research Institute of Structural Engineering and Disaster Reduction, Tongji University, Shanghai, China, 200092 (Corresponding author) E-mail: 08jzshan@tongji.edu.cn

[3] Graduate Student, Department of Mechanical Engineering, University of California, Santa Barbara, CA 93106, USA

[4] Professor, Department of Physics, University of California, Santa Barbara, CA 93106, USA

[5] Professor, Research Institute of Structural Engineering and Disaster Reduction, Tongji University, Shanghai, China

actual substructures to track the desired response signals. Result obtained by numerical simulations for the illustrative example in this study is further validated by experimental investigations employing a three-story aluminum frame structure. The asymptotically tracking of the state of the substructure and convergence of the time-varying parameters in the adaptive controller are found in agreement with experimental data obtained for this example. Several representative experimental data sets are compared with the corresponding numerical simulation results for this example with favorable correlations.

**CE Database subject headings**

Structural dynamics; Building structures; Adaptive control; Health monitoring; Earthquake

## INTRODUCTION

Structural vibration control and health monitoring of civil infrastructures during disastrous events such as strong earthquakes and winds have been actively investigated for several decades. Many notable vibration suppression technologies have been developed and applied for building structures. A comprehensive account of the research in the structural control of its past, present, and future was given by Housner *et al.* (1997). In parallel, many state-of-the-art health monitoring algorithms have been proposed, such as global vibration-based methods as summarized in the survey paper by Doebling *et al.* (1996) as well as on-line structural identification procedures (Yang and Lin 2005; Ghanem and Ferro 2006). While both structural control and health monitoring studies have mostly been done separately, both schools of studies are normally done in a way with complimentary goals in mind so that they can be integrated as one system.

Recently, the integration of health monitoring and vibration control has been investigated by several researchers. Schulz et al. (1999) presented techniques for monitoring the health and suppressing the vibration of flexible composite structures. Gattulli and Romeo (2000) presented an integrated procedure based on a direct adaptive control algorithm for robust control and damage detection of linear structural systems. An integrated procedure of vibration control and health monitoring of buildings structures with model updating using semi-active friction dampers has been proposed and numerically investigated (Chen and Xu 2008; Xu and Chen 2008). Nagarajaiah (2009) proposed an instantaneous frequency tracking control algorithm with smart tuned mass dampers.

The performance of traditional control design using time-invariant control gains may be significantly affected in the event of structural damage and long-term deterioration due to disastrous events and environmental loadings. In this regard, the adaptive structural control algorithms have been widely studied for structural engineering, as summarized by Utku and Wada (1993). One promising adaptive controller is the model-reference adaptive control , in which the desired performance was expressed in terms of a reference model (Astrom and Wittenmark 1995). A simple model-reference adaptive control method was proposed by Bar-Kana and Kaufman (1993) and was applied by several researchers (Hino *et al.* 1995; Bitaraf *et al.* 2012). Chu *et al.* (2010) presented an adaptive control application based on Lyapunov stability theory, and the control performance was numerically studied on a single degree-of-freedom structure.

In the previous studies, a series of global damage identification algorithms using displacement, velocity, or acceleration measurements have been presented by the research group of Yang and Hansma (Ma *et al.* 2005; Sebastijanovic *et al.* 2010; Lin *et al.* 2011), including, most recently, an interstory drift based method using acceleration feedback with decoupling technique was proposed for health monitoring (Shan *et al.* 2012). The damage tracking performance was experimentally investigated employing a three-story aluminum frame structure and a twelve-story concrete frame structure. In the interstory drift based acceleration feedback method, a virtual healthy structural system was defined by the parameters of the healthy structure. Meanwhile, a reference model is required in model-reference adaptive control. Therefore, it becomes possible to develop a hybrid structural health monitoring and control system containing two components, the previous interstory drift based acceleration feedback method and a model-reference

adaptive control algorithm. The virtual healthy structural system for health monitoring serves as the reference model for adaptive control.

In this paper, the concept of the hybrid structural health monitoring and control system is presented first with the illustration by a flow diagram. Then, the governing relations of a general structural system for both health monitoring and adaptive control are reported and discussed. A three-story shear beam model used in the previous health monitoring studies is investigated in the present numerical simulation section for model-reference adaptive control. An illustrative structure, a three-story aluminum structure with simulated stiffness changes, is built to experimentally study the performance of the hybrid structural health monitoring and control system. The experimental control performance of the present adaptive control algorithm, expressed in various forms such as control force, real-time updating of parameters, displacement and acceleration response, and state-tracking, are compared with those values obtained from numerical simulations with favorable agreement.

## HYBRID STRUCTURAL HEALTH MONITORING AND CONTROL SYSTEM

The concept and process of the hybrid structural health monitoring and control system is illustrated in Fig. 1. The first objective of the hybrid system is to detect the damage occurrence, location, and severity through an interstory based acceleration feedback method. As illustrated in Fig. 1, the damage occurrence and location are identified based on the real-time monitor output during the earthquake excitation, while the damage severity is estimated during the earthquake for future model updating. It must be noted that in order to emphasize the fundamental concept of integration of damage

monitoring and adaptive control, the illustrative example is focused on the three-story shear beam model. The research emphasizing correlation between the original complex structure and the equivalent simplified shear beam model for the purpose of repairing or retrofitting the damaged components and connections of the complex model after the earthquake remains to be studied and demonstrated in the future. The second objective of the hybrid system is to maintain the desired response defined from the pre-designed healthy reference model contained in the health monitors through the use of an actuator in the damaged region. The adaptive control force is generated through real-time updating of the parameters in the controller. The health monitoring and adaptive control are designed to be operated in parallel and in real time. This characteristic is different from several other hybrid systems which need model updating to connect the two components in sequential order. Therefore, the health monitoring and structural control delivery may be operated simultaneously in real time during earthquakes.

## FORMULATION

### *Decoupling of structural system*

A structural system such as a multistory building can commonly be modeled in extreme simplicity as a lumped-mass or shear-beam structure. The governing equation of such a linear model subjected to earthquake excitations can be written as

$$M\ddot{x} + C\dot{x} + \left(K + \Delta K\right)x = -Mh\ddot{x}_g + B_s U \tag{1}$$

where $x$ is the displacement vector; $\dot{x}$ and $\ddot{x}$ are the velocity and acceleration vectors, respectively; matrices $M$, $C$, and $K$ denote mass, damping, and stiffness matrices of the undamaged structure, respectively; $\ddot{x}_g$ is an excitation vector representing ground

acceleration distributed by the influence vector $h$; $U$ is the control force vector and distributed by the controller location matrix $B_s$; Matrix $\Delta K$ contains the information of the damage present in the structure. For a healthy structure, $\Delta K$ contains zeros. Equation (1) consists of a series of linear differential equations, which can be written generally as Eq. (2) and Eq. (3) from the force equilibrium consideration

$$\sum_{j=1}^{n} m_j \ddot{x}_j + c_1 \dot{x}_1 + \left(k_1 + \Delta k_1\right) x_1 = -\sum_{j=1}^{n} m_j \ddot{x}_g + u_1 \tag{2}$$

$$\sum_{j=i}^{n} m_j \ddot{x}_j + c_i \left(\dot{x}_i - \dot{x}_{i-1}\right) + \left(k_i + \Delta k_i\right)\left(x_i - x_{i-1}\right) = -\sum_{j=i}^{n} m_j \ddot{x}_g + u_i \,,\ n \geq i \geq 2 \tag{3}$$

where $n$ is the total number of degrees of freedom of the system, the lower cased letter $i$ denotes the floor number of the corresponding matrices or vectors, and $u_i$ is the control force on the $i^{\text{th}}$ story.

For generality and simplicity, the following formulations are based on Eq. (3), which can be written as

$$m_i\left(\ddot{x}_i - \ddot{x}_{i-1}\right) + c_i\left(\dot{x}_i - \dot{x}_{i-1}\right) + \left(k_i + \Delta k_i\right)\left(x_i - x_{i-1}\right) = -\sum_{j=i}^{n} m_j \ddot{x}_g - \sum_{j=i+1}^{n} m_j \ddot{x}_j - m_i \ddot{x}_{i-1} + u_i \tag{4}$$

Defining a new variable (interstory drift of the $i^{\text{th}}$ story) as

$$Y_i = x_i - x_{i-1} \tag{5}$$

and a nominal external force as

$$p_i = -\sum_{j=i}^{n} m_j \ddot{x}_g - \sum_{j=i+1}^{n} m_j \ddot{x}_j - m_i \ddot{x}_{i-1} \tag{6}$$

Equation (4) can then be written as

$$m_i \ddot{Y}_i + c_i \dot{Y}_i + k_i Y_i = p_i - \Delta k_i \left(x_i - x_{i-1}\right) + u_i \tag{7}$$

It is noted that when $i=1$, $Y_1 = x_1$, Eq. (7) becomes

$$m_1\ddot{Y}_1 + c_1\dot{Y}_1 + k_1 Y_1 = p_1 - \Delta k_1 x_1 + u_1 \ , \ p_1 = -\sum_{j=1}^{n} m_j \ddot{x}_g - \sum_{j=2}^{n} m_j \ddot{Y}_j \tag{8}$$

The variable $Y_i$ is the interstory drift of the corresponding story and has the same unit as $x_i$. The system described in Eq. (7) is equivalent to a lumped-mass model with one degree of freedom. Since no special or additional assumptions were made in deriving Eq. (7), all systems that can be described by Eqs. (2) and (3) can be reduced to single degree of freedom systems.

*Health monitoring*

Another characteristic observed from Eq. (7) is that among all the possible locations of damage $\left[\Delta k_1, ..., \Delta k_i, ... \Delta k_n\right]$ only $\Delta k_i$ affects this single degree of freedom system in Eq. (7) while the effects of damage on other stories are eliminated. Equations (7) and (8) correspond to the current state of the structure, which could be either damaged ($\Delta k_i \neq 0$) or undamaged ($\Delta k_i = 0$). For damage assessment, it is necessary to construct a virtual healthy system subjected to the same input excitation as a reference for comparison. The dynamic equation for this virtual healthy system can be expressed directly as

$$m_i\ddot{Y}_i + c_i\dot{Y}_i + k_i Y_i^r = p_i + u_i; \ i = 1 \sim n \tag{9}$$

where $Y_i^r$ denotes the interstory drift of the $i^{\text{th}}$ story of the virtual healthy system. Conceptually from the discussion above, structural damage represented by reduction in stiffness can be identified when the actual interstory responses $\left[\ddot{Y}_i, \dot{Y}_i, Y_i\right]$ deviates from

the estimated virtual responses $\left[\ddot{Y}_i, \dot{Y}_i, Y_i^r\right]$. Subtracting Eq. (7) from Eq. (9), the following response-damage relationship can be established:

$$m_i\ddot{r}_i + c_i\dot{r}_i + k_i r_i = \Delta k_i\left(x_i - x_{i-1}\right)$$

$$\ddot{r}_i = \ddot{Y}_i - \ddot{Y}_i, i = 2 \sim n \tag{10}$$

when $i = 1$, $$m_1\ddot{r}_1 + c_1\dot{r}_1 + k_1 r_1 = \Delta k_1 x_1$$

$$\ddot{r}_1 = \ddot{Y}_1 - \ddot{Y}_1 \tag{11}$$

The algorithms thus derived are applicable to all these kinds of the structural dynamic response measurements such as displacements, velocities and accelerations. For practicable engineering application, the quantity $\ddot{r}_i$ is chosen to be the weighted monitor output, which will generally be nonzero for a damage occurrence on the $i^{\text{th}}$ story when $\Delta k_i \neq 0$. The presence of the corresponding damage at a certain floor can be directly determined by examining the value of $\ddot{r}_i$ that is the output of the designed monitor.

Monitor output is normalized with respect to the measurements as given by the research group of the senior author (Ma *et al.* 2005; Sebastijanovic *et al.* 2010; Shan *et al.* 2012) as follows

$$\ddot{r}_{norm,i}\left(t\right) = \sqrt{\frac{\int_{t-t_h}^{t} \ddot{r}_i^2\left(\tau\right) d\tau}{\int_{t-t_h}^{t} \bar{y}_i^2\left(\tau\right) d\tau}} \tag{12}$$

where $\ddot{r}_{norm,i}$ is the normalized output for the $i^{\text{th}}$ monitor; $\ddot{r}_i$ is the output for the $i^{\text{th}}$ monitor; and $t_h$ denotes integration time horizon of past measurements used for normalization. Noting that $\bar{y}_i\left(t\right)$ equals to $\ddot{Y}_i = \ddot{x}_i - \ddot{x}_{i-1}$ $(i = 2 \sim n)$ and $\bar{y}_1\left(t\right) = \ddot{Y}_1 = \ddot{x}_1$.

Such normalized output is dimensionless and thus serves as a good indicator for stiffness changes.

*Model-reference adaptive control of the decoupled substructure*

To apply the model-reference adaptive control, Eq. (7) can be further written as

$$m_i \ddot{Y}_{pi} + c_{pi} \dot{Y}_{pi} + k_{pi} Y_{pi} = p_i + u_i \tag{13}$$

where $m_i$, $c_{pi}$, and $k_{pi}$ denote actual mass, damping, and stiffness of the $i^{\text{th}}$ story; $\left[\ddot{Y}_{pi}, \dot{Y}_{pi}, Y_{pi}\right]$ are the actual interstory responses. The acceleration measurement vector is defined as $\mathbf{w} = \left[\ddot{x}_g, \ddot{x}_1, \ddot{x}_2, ..., \ddot{x}_n\right]^T$. Then, the equation of the $i^{\text{th}}$ story can be reformulated into its state-space form as

$$\dot{\mathbf{X}}_{pi} = \mathbf{A}_{pi} \mathbf{X}_{pi} + \mathbf{B}_{pi} u_i + \mathbf{E}_{pi} \mathbf{w} \tag{14}$$

where

$$\mathbf{X}_{pi} = \begin{bmatrix} Y_{pi} \\ \dot{Y}_{pi} \end{bmatrix}_{2\times 1}, \mathbf{A}_{pi} = \begin{bmatrix} 0 & 1 \\ -k_{pi}/m_i, & -c_{pi}/m_i \end{bmatrix}_{2\times 2}, \mathbf{B}_{pi} = \begin{bmatrix} 0 \\ 1/m_i \end{bmatrix}_{2\times 1}$$

$$\mathbf{E}_{pi} = \begin{bmatrix} \mathbf{0}_{(n+1)\times 1} \\ -\sum_{j=i}^{n} m_j/m_i,\ 0...0, -1, 0, -m_{i+1}/m_i, ..., -m_n/m_i \end{bmatrix}_{(n+1)\times 2}$$

The virtual healthy system, previously adapted in Eq. (9), is designed to represent the reference model for model-reference adaptive control here. The equation of the reference model with healthy structural properties can be similarly formulated as

$$m_i \ddot{Y}_{mi} + c_{mi} \dot{Y}_{mi} + k_{mi} Y_{mi} = p_i \tag{15}$$

where $m_i$, $c_{mi}$, and $k_{mi}$ denote mass, damping, and stiffness of the "healthy" $i^{th}$ story; $\left[\ddot{Y}_{mi}, \dot{Y}_{mi}, Y_{mi}\right]$ are the interstory responses of the reference model. Equation (15) can be transformed into its state-space form as

$$\dot{\mathbf{X}}_{mi} = \mathbf{A}_{mi}\mathbf{X}_{mi} + \mathbf{E}_{mi}\mathbf{w} \tag{16}$$

where $\mathbf{X}_{mi} = \begin{bmatrix} Y_{mi} \\ \dot{Y}_{mi} \end{bmatrix}_{2\times 1}$, $\mathbf{A}_{mi} = \begin{bmatrix} 0 & 1 \\ -k_{mi}/m_i, & -c_{mi}/m_i \end{bmatrix}_{2\times 2}$, $\mathbf{E}_{mi} = \mathbf{E}_{pi}$. In Eqs. (14) and (16), the subscript $p$ and $m$ denote the actual controlled substructure and the corresponding reference model.

The adaptive feedback control law is designed as,

$$u_i = \theta_{di}Y_{pi} + \theta_{vi}\dot{Y}_{pi} = \boldsymbol{\theta}_i^T\mathbf{X}_{pi} \tag{17}$$

where $\boldsymbol{\theta}_i^T = \left[\theta_{di}, \theta_{vi}\right]_{1\times 2}$ is the time-varying adjustable feedback parameter vector. A sufficient condition for perfect tracking is that there exists a parameter value $\boldsymbol{\theta}_i^*$ as

$$\boldsymbol{\theta}_i^* = \begin{bmatrix} \theta_{di}^* \\ \theta_{vi}^* \end{bmatrix} = \begin{bmatrix} k_{pi} - k_{mi} \\ c_{pi} - c_{mi} \end{bmatrix} \tag{18}$$

The tracking-error is defined as

$$\boldsymbol{\eta}_i = \begin{bmatrix} e_i \\ \dot{e}_i \end{bmatrix} = \mathbf{X}_{pi} - \mathbf{X}_{mi} = \begin{bmatrix} Y_{pi} - Y_{mi} \\ \dot{Y}_{pi} - \dot{Y}_{mi} \end{bmatrix} \tag{19}$$

Subtracting Eq. (16) from Eq. (14) gives

$$\dot{\boldsymbol{\eta}}_i = \mathbf{A}_{mi}\boldsymbol{\eta}_i + \mathbf{L}\bar{\boldsymbol{\theta}}_i^T\mathbf{X}_{pi} \tag{20}$$

where $\mathbf{L} = \left[0,1\right]^T$, $\bar{\boldsymbol{\theta}}_i^T = \left(\boldsymbol{\theta}_i^T - \boldsymbol{\theta}_i^{*T}\right)/m_i$. To derive a parameter adjustment law, a quadratic Lyapunov function is introduced here as

$$V\left(\boldsymbol{\eta}_i, \bar{\boldsymbol{\theta}}_i\right) = \frac{1}{2}\left(\boldsymbol{\eta}_i^T \mathbf{P}_i \boldsymbol{\eta}_i + \bar{\boldsymbol{\theta}}_i^T \boldsymbol{\Gamma}_i^{-1} \bar{\boldsymbol{\theta}}_i\right) \tag{21}$$

where $\mathbf{P}_i$ is the $2\times 2$ positive-definite, symmetric adaptation matrix related to $\boldsymbol{\eta}_i$; and $\boldsymbol{\Gamma}_i = \mathrm{diag}\left(\left[\gamma_{i1}\ \gamma_{i2}\right]\right)$ is the positive-definite, symmetric diagonal adaptation matrix related to $\bar{\boldsymbol{\theta}}_i$. The time derivative of the defined Lyapunov function is calculated as

$$\dot{V}\left(\boldsymbol{\eta}_i, \bar{\boldsymbol{\theta}}_i\right) = -\frac{1}{2}\boldsymbol{\eta}_i^T \mathbf{Q}\boldsymbol{\eta}_i + \mathbf{X}_{pi}^T \bar{\boldsymbol{\theta}}_i \mathbf{L}^T \mathbf{P}_i \boldsymbol{\eta}_i + \dot{\bar{\boldsymbol{\theta}}}_i^T \boldsymbol{\Gamma}_i^{-1} \bar{\boldsymbol{\theta}}_i \tag{22}$$

where $\mathbf{Q}_i$ is positive definite and such that

$$\mathbf{P}_i \mathbf{A}_{mi} + \mathbf{A}_{mi}^T \mathbf{P}_i = -\mathbf{Q}_i \tag{23}$$

Notice that a pair of positive definite matrices $\mathbf{P}_i$ and $\mathbf{Q}_i$ always exist if $\mathbf{A}_{mi}$ is stable. It is noted that $\mathbf{X}_{pi}^T \bar{\boldsymbol{\theta}}_i$ and $\mathbf{L}^T \mathbf{P}_i \boldsymbol{\eta}_i$ are $1\times 1$ vectors. Therefore $\mathbf{X}_{pi}^T \bar{\boldsymbol{\theta}}_i \mathbf{L}^T \mathbf{P}_i \boldsymbol{\eta}_i = \mathbf{L}^T \mathbf{P}_i \boldsymbol{\eta}_i \mathbf{X}_{pi}^T \bar{\boldsymbol{\theta}}_i$. Equation (22) can be written as

$$\dot{V}\left(\boldsymbol{\eta}_i, \bar{\boldsymbol{\theta}}_i\right) = -\frac{1}{2}\boldsymbol{\eta}_i^T \mathbf{Q}\boldsymbol{\eta}_i + \mathbf{L}^T \mathbf{P}_i \boldsymbol{\eta}_i \mathbf{X}_{pi}^T \bar{\boldsymbol{\theta}}_i + \dot{\bar{\boldsymbol{\theta}}}_i^T \boldsymbol{\Gamma}_i^{-1} \bar{\boldsymbol{\theta}}_i \tag{24}$$

If the parameter adjustment law is chosen to be

$$\dot{\bar{\boldsymbol{\theta}}}_i^T = -\mathbf{L}^T \mathbf{P}_i \boldsymbol{\eta}_i \mathbf{X}_{pi}^T \boldsymbol{\Gamma}_i \tag{25}$$

then Eq. (24) can be written as a negative semi-definite function

$$\dot{V}\left(\boldsymbol{\eta}_i, \bar{\boldsymbol{\theta}}_i\right) = -\frac{1}{2}\boldsymbol{\eta}_i^T \mathbf{Q}\boldsymbol{\eta}_i \tag{26}$$

Therefore the derived adaptation law is

$$\dot{\boldsymbol{\theta}}_i = \begin{bmatrix} \dot{\theta}_{di} \\ \dot{\theta}_{vi} \end{bmatrix} = -m_i \begin{bmatrix} \gamma_{i1} Y_{pi}\left(P_{12} e_i + P_{22} \dot{e}_i\right) \\ \gamma_{i2} Y_{pi}\left(P_{12} e_i + P_{22} \dot{e}_i\right) \end{bmatrix} \tag{27}$$

where $P_{12}$ and $P_{22}$ are the first and second elements on the second column of $\mathbf{P}_i$. The model-reference adaptive control law for the $i^{\text{th}}$ story of the controlled structure is finally expressed in Eqs. (17) and (27). Furthermore, the asymptotically perfect tracking and convergence of adaptive gains are ensured based on the designed Lyapunov function.

*State-space form of health monitor*

The health monitor, as shown in Fig. 1, is designed to generate the monitor output from Eqs. (10) and (11) and the desired interstory response from Eq. (15). The state-space oriented description is adopted here to study the hybrid system rather than its counterpart described by higher order differential equations. The state vector is defined as $\mathbf{X}_i = \left[ Y_i^r, \dot{Y}_i, Y_{mi}, \dot{Y}_{mi} \right]_{1\times 4}^T$ for the $i^{\text{th}}$ story, the acceleration measurement vector is defined above as $\mathbf{w} = \left[ \ddot{Y}_g, \ddot{Y}_1, \ddot{Y}_2, ..., \ddot{Y}_n \right]_{1\times(n+1)}^T$, and the outputs of the state-space model is $\mathbf{y}_i = [\ddot{Y}_i, Y_{mi}, \dot{Y}_{mi}]_{1\times 3}^T$. Note that $\ddot{Y}_i$ are the story accelerations relative to the ground that can be straightforward obtained from the measured absolute accelerations. The equivalent state space representations of the health monitor corresponding to Eqs. (10), (11), and (15) can be obtained as follows

$$\begin{aligned} \dot{\mathbf{X}}_i &= \mathbf{A}_i \mathbf{X}_i + \mathbf{B}_i u_i + \mathbf{E}_i \mathbf{w} \\ \mathbf{y}_i &= \mathbf{C}_i \mathbf{X}_i + \mathbf{D}_i u_i + \mathbf{F}_i \mathbf{w} \end{aligned} \tag{28}$$

where

$$\mathbf{A}_i = \begin{bmatrix} 0 & 1 \\ -k_i/m_i, & -c_i/m_i \\ 0 & 1 \\ -k_i/m_i, & -c_i/m_i \end{bmatrix}_{4\times 2}, \mathbf{B}_i = \begin{bmatrix} 0 \\ 1/m_i \\ 0 \\ 0 \end{bmatrix}_{4\times 1}, \mathbf{C}_i = \begin{bmatrix} -k_i/m_i, & -c_i/m_i, & 0, & 0, \\ 0, & 0, & 1, & 0 \\ 0, & 0, & 0, & 1 \end{bmatrix}_{3\times 4}$$

$$\mathbf{D}_i = \begin{bmatrix} 1/m_i \\ 0 \\ 0 \end{bmatrix}_{3\times 1}, \mathbf{E}_i = \mathbf{E}_{pi}, \mathbf{F}_i = \begin{bmatrix} -\sum_{j=i}^{n} m_j / m_i,\ 0 \ldots 0, 0, -1, -m_{i+1}/m_i, \ldots, -m_n/m_i \\ \mathbf{0}_{(n+1)\times 1} \\ \mathbf{0}_{(n+1)\times 1} \end{bmatrix}_{3\times(n+1)}$$

Due to decoupling of damages at different locations, the health monitor is affected by the local damage in the corresponding monitoring region. Therefore, the following adaptive controller generates the control force after the occurrence of local damages, which deviates the monitored actual structure from the reference healthy model. This shows the local feedback control characteristic of the proposed control algorithm. Moreover, it is noted that the interstory drift and velocity need to be measurable for the adaptive control, as shown in Eqs. (17) and (27). The state estimators such as the Kalman filter is widely used for this practical limitation in traditional control algorithms. However, it may not be applicable here because of the assumption of damage indicating the unavailable pre-knowledge of the actual structure, which is required by the state estimators. It appears that measurement of interstory state, at least one of them, is inevitable. Currently, interstory drift is measurable in aftermentioned experimental study, and the corresponding interstory velocity is obtained through digital differential technique.

## NUMERICAL SIMULATION

The illustrative model considered was a three-story shear beam model corresponding to a three-story frame structure presented by Yang *et al.* (1995). The mass, stiffness and damping parameters of each floor were assumed as 1,000kg, 980kN/m, and 1.407kN-s/m, respectively. The damage of each floor was defined as changes in the equivalent stiffness

coefficients as in the previous studies (Ma *et al.* 2005). The severity of the damage was simplified and indicated by the percentage of stiffness changes $\alpha_i$, where $i$ denotes story number. For the original undamaged model, $\alpha_i = 0$. The north-south (N-S) component of the ground acceleration of the 1940 El Centro earthquake was used as an excitation source for the present models with an amplitude of $200\,cm/s^2$. The measurement noise was assumed to have a signal-to-noise-ratio (SNR) of 30 dB.

Three cases, similar to that in the previous study (Ma *et al.* 2005), were assumed for the three-story model. For the undamaged model (case 1), the values of $\alpha_1$, $\alpha_2$, and $\alpha_3$ were all at 0. For case 2, there was a sudden stiffness change during the excitation in $\alpha_3$ from 0 to 15% at onset of the fifth second, while $\alpha_1 = \alpha_2 = 0$ for the entire time history. The values of $\alpha_1$, $\alpha_2$, and $\alpha_3$ were chosen as 40%, 20% and 20%, respectively in case 3 as a damaged model. Three health monitors were placed to the decoupled three single degree of freedom subsystems corresponding to the three stories. The integration time horizon $t_h$ defined in Eq. (12) was chosen to be 4.0 seconds for this particular study. For every decoupled single degree of freedom system, the adaptation weighting matrix $\mathbf{\Gamma}$ of model-reference adaptive control was assumed the same as

$$\mathbf{\Gamma}_{1,2,3} = \begin{pmatrix} 100 & 0 \\ 0 & 100 \end{pmatrix} \tag{29}$$

while the symmetric positive-definite matrix $\mathbf{Q}$ was defined as

$$\mathbf{Q}_{1,2,3} = 100 \begin{pmatrix} 1 & 0 \\ 0 & 1 \end{pmatrix} \tag{30}$$

and substituted it into Eq. (23). The corresponding matrix can be uniquely obtained as

$$\mathbf{P}_{1,2,3} = \begin{pmatrix} 3486 & 0.0051 \\ 0.0051 & 3.5573 \end{pmatrix} \tag{31}$$

The initial conditions of $\theta_d$ and $\theta_v$ were $\theta_d(t=0) = \theta_v(t=0) = 0$. With the parameters determined above, the adaptation mechanism in Eq. (27) and the adaptive controller in Eq. (17) of the model-reference adaptive control algorithm can be applied on the three floors.

The health monitoring performance of the hybrid system using the previously proposed interstory drift based acceleration feedback method is illustrated in Fig. 2. The original and normalized monitor output for the first and second floor, as illustrated in Figs. 2(b), (c), (e), and (f), are stable and not distinguishable between case 1 and 2 indicating the similar stiffness conditions. The stiffness change as applied on the third floor from 0 to 15% at onset of the fifth second is noticeably identified by both the sudden jump in original monitor output and also that in the normalized monitor output in Figs. 2(a) and (d), respectively. The effects of three assigned values in stiffness change on the three floors in case 3 have been noticeably identified in the monitor output in Figs. 2(a, b, c) and especially in the normalized monitor output in Figs. 2(d, e, f).

The control performance in cases 2 and 3, containing peak and root-mean-square (RMS) values of responses and maximum control forces, is listed in Table 1. The RMS response quantities within the time duration $t_f$ are calculated by $x_{rms} = \sqrt{\frac{1}{t_f}\int_0^{t_f} x(t)^2\, dt}$. The peak and RMS values of the response of the assumed uncontrolled damaged structure are slightly and apparently increased in case 2 and 3, respectively. For example, the 15% stiffness reduction on the third floor at $t \geq 5$ seconds results in a 7.4% increase of peak displacement on the same floor from 5.29 *cm* to 5.68 *cm*, while the 40%, 20%, and

20% stiffness changes in case 3 on the three floors, respectively, lead to roughly 68.1%, 50.8%, and 47.4% increases in peak displacement, i.e., from 2.45 *cm*, 4.31 *cm*, and 5.29 *cm* to 4.12 *cm*, 6.50 *cm*, and 7.80 *cm*, respectively. In view of these undesirably large structural responses due to the assumed damages, it is of interest to examine the effect of the currently developed model-reference adaptive control method in generating the control forces required to suppress them to the desirable level.

For case 2, it is shown in Table 1 that the amplitude of control force has increased significantly to 560 *N* on the third floor while remaining at relatively low levels on the other two floors (30.4 *N* and 29.3 *N*, respectively). This indicates that damage occurrence will lead to an increase in the actuating force of the corresponding floor while have little effect on the actuators on the other undamaged floors, showing the characteristic of local feedback control of the proposed control algorithm for this example. Figure 3 shows the time histories of the two time-varying adjustable parameters and the corresponding control forces on the third floor. It is observed that the parameters started updating after the prescribed damage occurrence at the onset of the fifth second, resulting in a noticeable increases in the adaptive control force after the damage occurrence. This example illustrates the time history behavior of the forces generated by the currently proposed model-reference adaptive control algorithm as a result of the occurrence of the assumed level of damages.

Figure 4 illustrates the displacement and acceleration responses between model-reference adaptive controlled and uncontrolled structures in case 3, while Fig. 5 shows the time history of corresponding control force on the three respective floors. The sets of time history curves in Fig. 4 show the behaviors that the present control algorithm is able

to perform in terms of suppressing the undesirable dynamic response of the structure with the damage occurrence as assumed in case 3. Figure 5(b) and (c) show that the actuating forces are significantly increased when the 40% and 20% stiffness changes are assigned to the first and second floor, respectively, with the control forces on Floor 1 being almost order of magnitude larger than that on Floor 2.

For illustrative purpose, the first floor with the maximum assigned stiffness change is selected to show the performance of the model-reference adaptive control. The updating profiles of the adjustable parameters $\theta_{d1}$ and $\theta_{v1}$ are shown in Fig. 6(a) and (b), respectively. The real-time calculated desired displacement response of the undamaged model and the actual controlled displacement response of the damaged model on the first floor are shown in Fig. 6(c) to show the displacement tracking performance. The convergence plots of $\theta_{d1}$ and $\theta_{v1}$ are illustrated in Fig. 6(a) and (b), respectively. The two parameters roughly converge to the stable levels after fifth second. Similarly, it is observed in Fig. 6(c) that the actual controlled response curve is relatively undistinguishable from the desired response curve after the initial significant decaying of $\theta_{d1}$ and $\theta_{v1}$ around fifth second. This indicates that the present adaptive control algorithm will exhibit its control performance as intended after the real-time convergence of the parameters. The observation here in Fig. 6 also explains the time history effect of control forces on displacement and acceleration after fifth second as shown in Fig. 4.

## EXPERIMENTAL VALIDATION

### *Experimental description and results*

A three-story aluminum structure, as shown in Fig. 7(a), was built in the Hansma research laboratory at University of California, Santa Barbara, for the experimental validation of the proposed hybrid system. Four aluminum solid rods with diameter of $0.9cm$ and height of $1.68m$ were used as the four corner columns, and three aluminum rectangular plates was used as the two floors and the roof, each with dimensions of $0.61m$, $0.51m$, and $1.3cm$ for length, width, and thickness, respectively. The mass of each floor was 11.09 $kg$. The structural damage was assumed as the interstory stiffness change on the first floor, which was generated using a spring attachment as shown in Fig. 7(b). The healthy structure was considered at the state with the attached springs with a stiffness of $773.5\,N/m$ for the present example. Thus the reduction of stiffness from this level could be assumed as due to damage. An active actuator was developed which consisted of a voice coil mounted to a linear translation stage. The actuator was placed on the first floor to provide the required control force based on the adaptive control algorithm. Figure 7(b) illustrates the spring device and the active actuator installed on the first floor. The base of the actuator and spring system was fixed rigidly to the ground floor. The experimental structure was subjected to the 1940 El Centro earthquake (N-S component) by a unidirectional shaking table. The time interval of the excitation was 0.004 seconds, and the peak acceleration of the input was $0.1g$. The horizontal displacement and acceleration responses in loading direction were measured on the ground and three upper floors. Two sets of stiffness scenarios with different control states were conducted and summarized in Table 2.

As a linear lumped-mass model, the interstory stiffness of the three-story symmetric structure in stiffness scenario I was identified as $k_1 = 6625\,N/m$, $k_2 = 7000\,N/m$,

$k_3 = 7100\,N/m$ for the three respective floors. Figure 8 shows the time history responses of the numerical simulation using the analytical model, and those of the experimental structure in scenario I. Close correlation between the numerical calculations and experimental measurements were observed in displacement and acceleration at all these floors. The increased interstory stiffness to the first floor by the attached springs experimentally was estimated as $\Delta k_1 = 773.5\,N/m$ for stiffness scenario I, so the corresponding percent stiffness reduction in $\alpha_1$ was 11.7% for stiffness scenario II.

The integration time horizon $t_h$ was assigned as 4 seconds beforehand for health monitoring for the present example. The reference model for the adaptive control algorithm for the first floor was developed from the identified structural parameters in stiffness scenario I. The corresponding $\mathbf{A}_{m1}$ for the first floor was then determined as

$$\mathbf{A}_{m1} = \begin{pmatrix} 0 & 1 \\ -597.34 & -1.9836 \end{pmatrix} \tag{32}$$

For the decoupled substructure representing the first floor, the adaptation weighting matrix $\mathbf{\Gamma}$ and the symmetric positive-definite matrix $\mathbf{Q}$ of the model-reference adaptive control algorithm were defined as

$$\mathbf{\Gamma}_1 = \begin{pmatrix} 10 & 0 \\ 0 & 2 \end{pmatrix},\ \mathbf{Q}_1 = \begin{pmatrix} 10^7 & 0 \\ 0 & 10^3 \end{pmatrix} \tag{33}$$

The corresponding matrix can be uniquely obtained from Eq. (23) as

$$\mathbf{P}_1 = 1000 \begin{pmatrix} 2687.81 & 8.37 \\ 8.37 & 4.47 \end{pmatrix} \tag{34}$$

The initial conditions were set as $\theta_d(t=0)=\theta_v(t=0)=0$. The interstory drift of the first floor was directly measured during the experiment, while the interstory velocity was real-time calculated through digital differential technology.

Figure 9 shows the tracking results of different stiffness scenarios. In Fig. 9(f), the normalized monitor output shows that the damaged and the undamaged scenarios are readily distinguishable to each other. The normalized monitor output, as shown in Figs. 9(d) and (e), for the second and third floor, respectively, remain stable and similar in different stiffness scenarios indicating the similar stiffness condition on the second and third floor. Previously, a damage severity estimation method utilizing numerical prediction curve of stiffness change with linear interpolation technique was presented and experimentally verified (Shan *et al.* 2012). The numerical prediction curve of the three-story structure in this study with the SNR of 30 dB is plotted in Fig. 10. The discrete values of the prediction curve are calculated from pre-set stiffness changes $\alpha_i = 0, 1, 5, 10, \text{L } 25$. For example, the mean value of the normalized monitor output from numerical model with $\alpha_1 = 0$ is 0.052, while that from numerical model with assumed $\alpha_1 = 10\%$ is 0.123. Therefore, the difference of normalized monitor output for the 10% stiffness change on the first floor is 0.071, which is marked as point A in Fig. 10. For illustrative purpose, the normalized monitor output in stiffness scenario I and stiffness scenario II with adaptive control were selected. The calculated $\Delta\overline{\ddot{\theta}}_{norm,i}$ from the experimental measurement is 0.104, which predicts the $\alpha_{1,prediction}$ being 13.0%, as shown in Fig. 10. The experimentally applied 11.7% and the predicted 13.0% stiffness change

are in fair agreement. However, there is a slight discrepancy that may be due to measurement noise.

In addition to the illustration of health monitoring performance, the control performance of model-reference adaptive control for local feedback is investigated in this section. The control performance indices on vibration control of the assumed damaged structure can be illustrated by comparing peak and RMS responses as listed in Table 3. For the uncontrolled cases as listed in Table 3, the peak response of the damaged structure increased approximately 15%~27% for displacement and acceleration, except for the acceleration on the second floor. Meanwhile, the peak responses of the adaptive-controlled structure in stiffness scenario II are effectively suppressed as compared to those without control, roughly 16~18% and 7~18% improvement in displacement and acceleration, respectively. In terms of RMS response, the present control algorithm shows approximately 40~41% and 38~39% reduction of displacement and acceleration, respectively.

*Comparison of results between experimental aluminum structure and numerical simulation model*

In the proposed model-reference adaptive control algorithm, the online updating and asymptotical convergence of the time-varying adjustable feedback parameters $\theta_d, \theta_v$ are important to generate the required active control force for model-reference state tracking. The discrete instantaneous values of $\theta_d, \theta_v$ were saved during the experiment. The time histories of $\theta_d, \theta_v$ both from experimental structure and numerical simulation are illustrated and compared in Fig. 11. The asymptotical convergence curves for cases

reached good agreement after 4 seconds both experimentally and numerically as shown in Fig. 11. Close correlation of the updating process and the final convergence seems to have reached between the present experimental structure and numerical model. Figure 12 shows the time history responses between the numerical simulation and the experimental measurement for stiffness scenario II ($\alpha_1 = 11.7\%, \alpha_2 = \alpha_3 = 0$) with adaptive control implementation. It is shown that the agreements in displacement and acceleration responses are excellent. The time histories of the experimental control force delivered by actuator, commanded by adaptive controller, and predicted by numerical simulation are also shown in Fig. 13. The periodic oscillating of the time history curves are observed as nearly the same for all the three curves.

Besides the comparison of peak and RMS responses in traditional control techniques, state tracking performance study provides an additionally distinguishable way of investigation for the proposed model-reference adaptive control algorithm. Figure 14 shows the experimental and numerical tracking performance of the interstory drift on the first floor. Although the convergence becomes roughly stable after the fourth second as shown in Fig. 12, its asymptotical tracking performance, between the calculated response of undamaged model and actually controlled response of damaged model, is excellent through the entire time history both in experimental structure and numerical simulation.

## PARAMETRIC STUDY

It is noted that although the desirable levels of controllable reduction in peak and RMS displacement and acceleration can be achieved by the present proposed method, however, achieving these goals are at the expenses of the achievable active control forces.

It is of interest to perform a preliminary parametric study numerically on the relation between control forces and resulting controlled responses. The present illustrative three-story shear beam model subjected to the N-S component of the ground acceleration of the 1940 El Centro earthquake was used again for the parametric study. The stiffness change ($\alpha_1$) on the first floor was assumed as 20% and 40% in two separate cases, while these stiffness change $\alpha_2$ and $\alpha_3$ on the second and third floor, respectively, were assumed as undamaged. The diagonal elements of the adaptation weighting matrix $\mathbf{\Gamma}$ was adjusted from 0.1 to 10000 to achieve different levels of control force output. As shown in Fig. 6(c) by numerical simulation and Fig. 14 by experimental validation, the state tracking performance is a way of identifying the levels of achievement by the adaptive control. It is proposed that the ratio between controlled interstory drift of damaged floor and interstory drift of original reference healthy floor in the form of RMS value, be called, for lack of a better term, "recovery factor", This recovery factor is now used to evaluate the state tracking performance. In an ideal situation, the recovery factor is expected to be brought to unity when perfect state tracking is achieved, i.e. the interstory drift of the damaged floor is controlled to be the same as that of original undamaged floor. In reality, this value could be brought down to be below unity, although it may be viewed as undesirable in terms of the currently assumption, using the undamaged model as the reference state and the desired achievable goal

Figure 15(a) shows the relation between the controlled interstory drifts of the damaged first floor and the corresponding control forces on the same floor, and Fig. 15(b) shows the relation between the recovery factors and the control forces. It is seen that controlled drift response and corresponding recovery factor decrease when control force

increases. The increase of control force at relatively low magnitudes (0~300 *N*) shows more rapid improvement on the controlled drift response than that at relatively high magnitudes (600~900 *N*). Conversely, recovery factor shows more rapid improvement in RMS controlled force at relatively high magnitudes (600~900 *N*) than that at relatively low levels (0~300 *N*).

## CONCLUSION

A model-reference adaptive control algorithm integrated with a structural decoupling technique for local feedback control has been discussed in the paper. A hybrid structural health monitoring and control system is then introduced with integration of the previous interstory drift acceleration feedback method and the model-reference adaptive control algorithm. The real-time health monitoring and control performance of the proposed hybrid system has been numerically investigated and experimentally validated employing a three-story aluminum frame structure with an active control system. It is shown that the damage of each floor would only affect the corresponding health monitor and lead to the actuating on the corresponding floor. The asymptotically tracking of state of the substructure and convergence of time-varying adjustable parameters in controller are favorably compared through the experimental study of the current three floor model. The updating and convergence of the time-varying feedback parameters, the dynamic responses, the adaptive control force, and the state-tracking performance from the numerical simulations are validated by the experiment with favorable correlations for the current 3-story example. The concept of the structural health monitoring may be integrated with control system in real time during the earthquake excitation as proposed

in the flow diagram in Fig. 1. To conclude in the illustration of the proposed integrated closed-loop system, a self-contained figure with an example of the current three story structure subjected to El Centro earthquake is finally shown in Fig. 16. The currently proposed hybrid real time structural health monitoring and control system may contribute to the integrated sensing and control technology of future smart structures.

Currently, this proposed hybrid system, as shown in Fig. 1, is only applicable to detect damages of certain floors in simplified model instead of damage in certain structural components or connections in original complex model. A logical next step seems to further develop the current numerical simulation method to refer back from simplified model to complex finite element model of the original full building so that the damage assessed and located could be controlled and even repaired at the level of structural components and connection. Another logical next step seems to develop a hybrid system to replace active controllers by adaptive passive controllers in the process as described in Fig. 1. It is noted that an innovative bio-inspired actuator simulating the mechanism of abalone shell or bones as developed by the current research team could be used for this study (Yang *et al.* 2010).

ACKNOWLEDGEMENTS

This study is sponsored by the National Science Foundation grant CMS 1014958, and the support of program director, Bruce M. Kramer, is gratefully acknowledged. Fellowship from the China Scholarship Council for one of the authors' work at University of California, Santa Barbara, is acknowledged.

REFERENCES

Astrom, K. J., and Wittenmark, B. (1995). *Adaptive Control, 2nd edition*, Addison-Wesley.

Bar-Kana, I., and Kaufman, H. (1993). "Simple adaptive control of large flexible space structures." *Aerospace and Electronic Systems, IEEE Transactions on*, 29(4), 1137-1149.

Bitaraf, M., Hurlebaus, S., and Barroso, L. R. (2012). "Active and Semi-active Adaptive Control for Undamaged and Damaged Building Structures Under Seismic Load." *Computer-Aided Civil and Infrastructure Engineering*, 1-17 (DOI: 10.1111/j.1467-8667.2011.00719.x).

Chen, B., and Xu, Y. (2008). "Integrated vibration control and health monitoring of building structures using semi-active friction dampers: Part II—Numerical investigation." *Engineering Structures*, 30(3), 573-587.

Chu, S. Y., Lo, S. C., and Chang, M. C. (2010). "Real-time control performance of a model‐reference adaptive structural control system under earthquake excitation." *Structural Control and Health Monitoring*, 17(2), 198-217.

Doebling, S. W., Farrar, C. R., Prime, M. B., and Shevitz, D. W. (1996). "Damage identification and health monitoring of structural and mechanical systems from changes in their vibration characteristics: a literature review." Los Alamos National Lab., NM (United States).

Gattulli, V., and Romeo, F. (2000). "Integrated procedure for identification and control of MDOF structures." *Journal of Engineering Mechanics*, 126(7), 730-737.

Ghanem, R., and Ferro, G. (2006). "Health monitoring for strongly non‐linear systems using the Ensemble Kalman filter." *Structural Control and Health Monitoring*, 13(1), 245-259.

Hino, M., Iwai, Z., Mizumoto, I., and Kohzawa, R. (Year). "Active vibration control of a multi-degree-of-freedom structure by the use of decentralized simple adaptive control." Proceedings of the 4th IEEE Conference on Control Applications, 1067-1072.

Housner, G., Bergman, L., Caughey, T., Chassiakos, A., Claus, R., Masri, S., Skelton, R., Soong, T., Spencer, B., and Yao, J. (1997). "Structural control: past, present, and future." *Journal of Engineering Mechanics*, 123(9), 897-971.

Lin, C. H., Sebastijanovic, N., Yang, H. T. Y., He, Q., and Han, X. (2011). "Adaptive structural control using global vibration sensing and model updating based on local infrared imaging." *Structural Control and Health Monitoring*, (Published online), DOI: 10.1002/stc.458.

Ma, T. W., Yang, H. T. Y., and Chang, C. C. (2005). "Structural damage diagnosis and assessment under seismic excitations." *Journal of Engineering Mechanics*, 131(10), 1036-1045.

Nagarajaiah, S. (2009). "Adaptive passive, semiactive, smart tuned mass dampers: identification and control using empirical mode decomposition, hilbert transform, and shor-term fourier transform." *Structural Control and Health Monitoring*, 16, 800-841.

Schulz, M., Pai, P., and Inman, D. (1999). "Health monitoring and active control of composite structures using piezoceramic patches." *Composites Part B: Engineering*, 30(7), 713-725.

Sebastijanovic, N., Yang, H. T. Y., and Ma, T. W. (2010). "Detection of changes in global structural stiffness coefficients using acceleration feedback." *Journal of Engineering Mechanics*, 136(9), 1187-1191.

Shan, J. Z., Yang, H. T. Y., Shi, W. X., Bridges, D., and Hansma, P. K. (2012). "Structural Damage Diagnosis Using Interstory Drift Based Acceleration Feedback with Test Validation." *Journal of Engineering Mechanics*, (Published online), DOI: 10.1061/(ASCE)EM.1943-7889.0000531.

Utku, S., and Wada, B. K. (1993). "Adaptive structures in Japan." *Journal of intelligent material systems and structures*, 4(4), 437-451.

Xu, Y., and Chen, B. (2008). "Integrated vibration control and health monitoring of building structures using semi-active friction dampers: Part I—methodology." *Engineering Structures*, 30(7), 1789-1801.

Yang, H. T. Y., Lin, C. H., Bridges, D., Randall, C. J., and Hansma, P. K. (2010). "Bio-inspired passive actuator simulating an abalone shell mechanism for structural control." *Smart Materials and Structures*, 19, 105011.

Yang, J. N., and Lin, S. (2005). "Identification of parametric variations of structures based on least squares estimation and adaptive tracking technique." *Journal of Engineering Mechanics*, 131(3), 290-298.

Yang, J. N., Wu, J. C., and Agrawal, A. K. (1995). "Sliding mode control for seismically excited linear structures." *Journal of Engineering Mechanics*, 121(12), 1386-1390.

**Table list**

**Table 1.** Comparison on control performance of the three-story numerical model in different cases

| Index | Floor No | Case 1 | Case 2 | | Case 3 | |
|---|---|---|---|---|---|---|
| | | Uncontrolled | Uncontrolled | Controlled | Uncontrolled | Controlled |
| Peak of displacement (cm) | 1 | 2.45 | 2.54 | 2.39 | 4.12 | 2.96 |
| | 2 | 4.31 | 4.48 | 4.20 | 6.50 | 4.62 |
| | 3 | 5.29 | 5.68 | 5.43 | 7.80 | 5.51 |
| Peak acceleration ($m/s^2$) | 1 | 5.71 | 5.89 | 5.91 | 5.83 | 4.60 |
| | 2 | 8.55 | 9.21 | 7.74 | 8.52 | 6.22 |
| | 3 | 10.56 | 11.05 | 10.40 | 10.20 | 6.92 |
| RMS of displacement (cm) | 1 | 0.69 | 0.69 | 0.58 | 0.85 | 0.38 |
| | 2 | 1.24 | 1.24 | 1.05 | 1.35 | 0.60 |
| | 3 | 1.54 | 1.61 | 1.35 | 1.62 | 0.72 |
| RMS of acceleration ($m/s^2$) | 1 | 1.38 | 1.35 | 1.16 | 1.15 | 0.53 |
| | 2 | 2.40 | 2.37 | 2.02 | 1.77 | 0.79 |
| | 3 | 2.99 | 3.07 | 2.58 | 2.13 | 0.96 |
| Peak force (N) | 1 | / | / | 30.44 | / | 2296.08 |
| | 2 | / | / | 29.34 | / | 277.85 |
| | 3 | / | / | 559.92 | / | 45.61 |

**Table 2.** Summary of the experimental setup

| Stiffness scenario | Attached stiffness (N/m) | Time length (sec) | Sampling frequency (Hz) | Defined condition | Control state |
|---|---|---|---|---|---|
| I | 773.5 | 10.53 | 250 | Healthy | Uncontrolled |
| II | 0 | 10.53 | 250 | Damaged | Uncontrolled |
| II | 0 | 10.53 | 250 | Damaged | Adaptive controlled |

**Table 3.** Comparison of the peak and RMS response of the three-story structure

| Stiffness scenario | Floor | I (Uncontrolled) | | II (Uncontrolled) | | II (Controlled) | |
|---|---|---|---|---|---|---|---|
| Index | No | Test | Calculation | Test | Calculation | Test | Calculation |
| Peak of | 1 | 0.45 | 0.47 | 0.58 | 0.50 | 0.47 | 0.47 |
| displacement | 2 | 0.76 | 0.82 | 0.93 | 0.83 | 0.77 | 0.80 |
| (cm) | 3 | 1.04 | 0.99 | 1.20 | 1.07 | 0.97 | 0.99 |
| Peak of | 1 | 1.35 | 1.38 | 1.57 | 1.40 | 1.44 | 1.36 |
| acceleration | 2 | 1.64 | 1.51 | 1.63 | 1.41 | 1.36 | 1.27 |
| ($m/s^2$) | 3 | 1.66 | 1.55 | 2.09 | 1.56 | 1.72 | 1.58 |
| RMS of | 1 | 0.18 | 0.21 | 0.26 | 0.26 | 0.16 | 0.18 |
| displacement | 2 | 0.30 | 0.37 | 0.45 | 0.45 | 0.26 | 0.31 |
| (cm) | 3 | 0.41 | 0.46 | 0.59 | 0.54 | 0.35 | 0.38 |
| RMS of | 1 | 0.32 | 0.34 | 0.48 | 0.43 | 0.30 | 0.29 |
| acceleration | 2 | 0.47 | 0.49 | 0.64 | 0.58 | 0.39 | 0.38 |
| ($m/s^2$) | 3 | 0.53 | 0.58 | 0.73 | 0.66 | 0.45 | 0.46 |
| Force | | / | | / | | 1.94 | 1.44 |

**Figure list**

**Figure 1.** Schematic diagram of the hybrid structural health monitoring and control system combining acceleration feedback method and model-reference adaptive control

**Figure 2.** Damage identification for different scenarios of the three-story numerical model: (a)-(c) are original monitor output for case 1-3; (d)-(f) are normalized monitor output for case 1-3, where in case 1: $\alpha_1 = \alpha_2 = \alpha_3 = 0$; case 2: $\alpha_1 = \alpha_2 = 0$, $\alpha_3 = 0$ at $t < 5\,\text{sec}$, $\alpha_3 = 15\%$ at $t \geq 5\,\text{sec}$; case 3: $\alpha_1 = 40\%$, $\alpha_2 = 20\%$, $\alpha_3 = 20\%$

**Figure 3.** Time history of two time-varying adjustable parameters and the corresponding control forces on the third floor in case 2

**Figure 4.** Comparison of response time histories of the three floors in case 3, with (a)-(c) for displacements, and (d)-(f) for accelerations on the three respective floors

**Figure 5.** Time history of control forces on the three respective floors in case 3

**Figure 6.** Shown in (a) and (b) are the time histories of two time-varying adjustable parameters, and shown in (c) are the calculated displacement responses of undamaged model and actual controlled displacement response of damaged model on the first floor in case 3

**Figure 7.** (a) The experimental three-story aluminum frame structure; (b) The active actuator and stiffness change device installed to the first floor of the three-story aluminum structure. The components of this system comprise of: A-force transducer, B-active actuator, C-attached springs, and D-first floor plane;

**Figure 8.** Comparison of the dynamic responses between the numerical simulation and experimental measurement of the three story aluminum model in scenario I (uncontrolled and $\alpha_1 = \alpha_2 = \alpha_3 = 0$) subjected to 1940 El Centro earthquake (N-S component), with (a)-(c) for displacements, and (d)-(f) for accelerations on the three respective floors

**Figure 9.** Original and normalized monitor output for three-story experimental structure in different stiffness scenarios: (a)-(c) are original monitor output, and (d)-(f) are normalized monitor output for scenario I ($\alpha_1 = \alpha_2 = \alpha_3 = 0$), II ($\alpha_1 = 11.7\%$, $\alpha_2 = \alpha_3 = 0$), respectively

**Figure 10.** A numerical prediction curve for the first floor of the three-story structure using a linear interpolation prediction approach to predict the stiffness values in stiffness scenario II ($\alpha_1 = 11.7\%,\ \alpha_2 = \alpha_3 = 0$) with control implementation

**Figure 11.** Comparison of updating and convergence of time-varying adjustable feedback parameters $\theta_d, \theta_v$ between experimental structure and numerical model

**Figure 12.** Comparison of the dynamic responses between numerical simulation and experimental measurement in stiffness scenario II ($\alpha_1 = 11.7\%$, $\alpha_2 = \alpha_3 = 0$) with adaptive control implementation under 1940 El Centro earthquake (N-S component), with (a)-(c) for displacements, and (d)-(f) for accelerations on the three respective floors

**Figure 13.** Comparison of the time history of the control force between experimental measurement and numerical simulation

**Figure 14.** Experimental and numerical tracking performance of displacement on the first floor in stiffness scenario II ($\alpha_1 = 11.7\%,\ \alpha_2 = \alpha_3 = 0$) with adaptive control

**Figure 15.** Parametric study: (a) is the relation between controlled interstory drifts and control forces in form of RMS value; (b) is the relation between recovery factors and RMS values of control force

**Figure 16.** Illustration of the hybrid structural health monitoring and control system as given in Fig. 1 using the case 2 ($\alpha_1 = \alpha_2 = 0,\ \alpha_3 = 0$ at $t < 5\,\text{sec}$, $\alpha_3 = 15\%$ at $t \geq 5\,\text{sec}$) in numerical simulation section shown in Figs 2 and 3

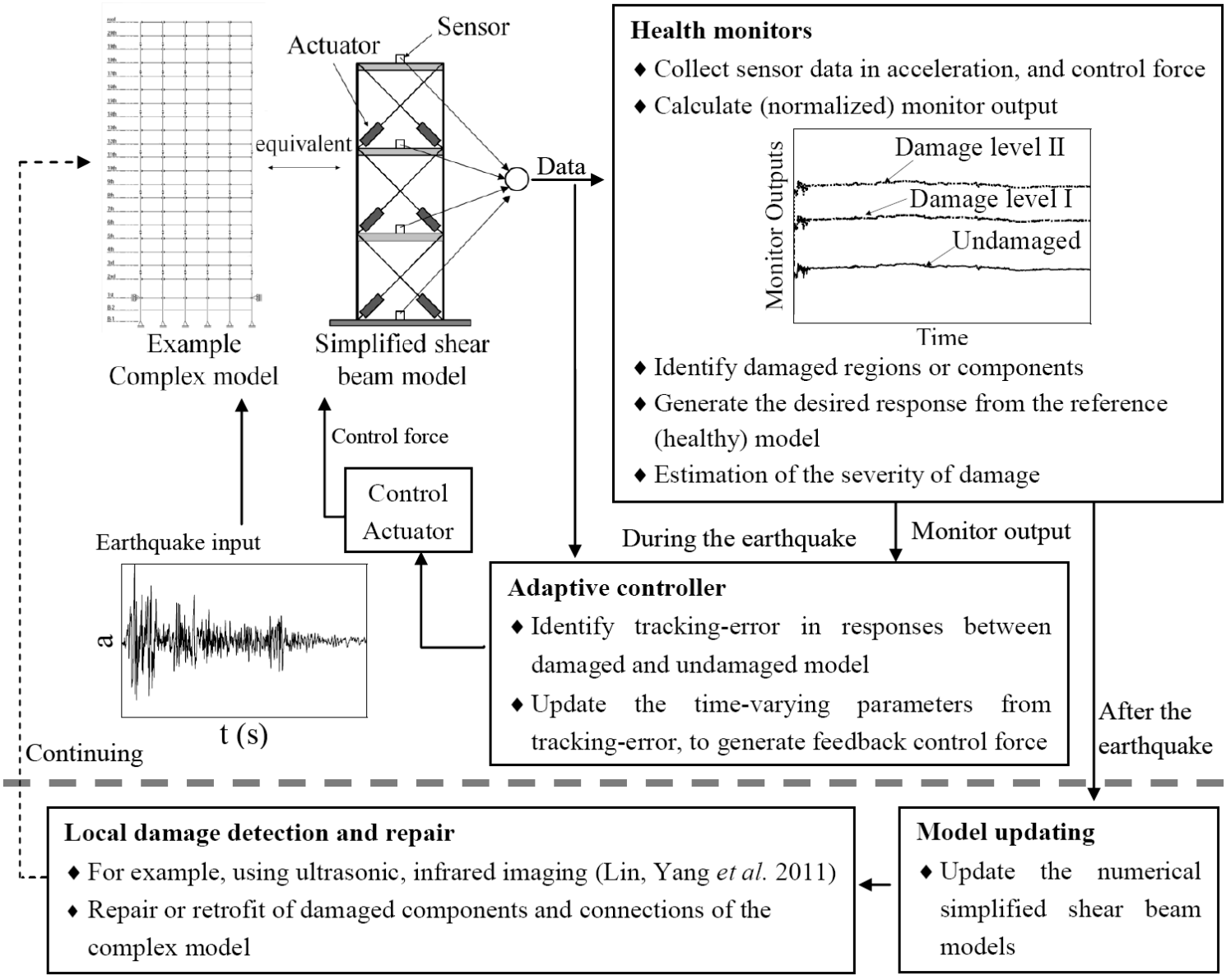


**Figure 1.** Schematic diagram of the hybrid structural health monitoring and control system combining acceleration feedback method and model-reference adaptive control

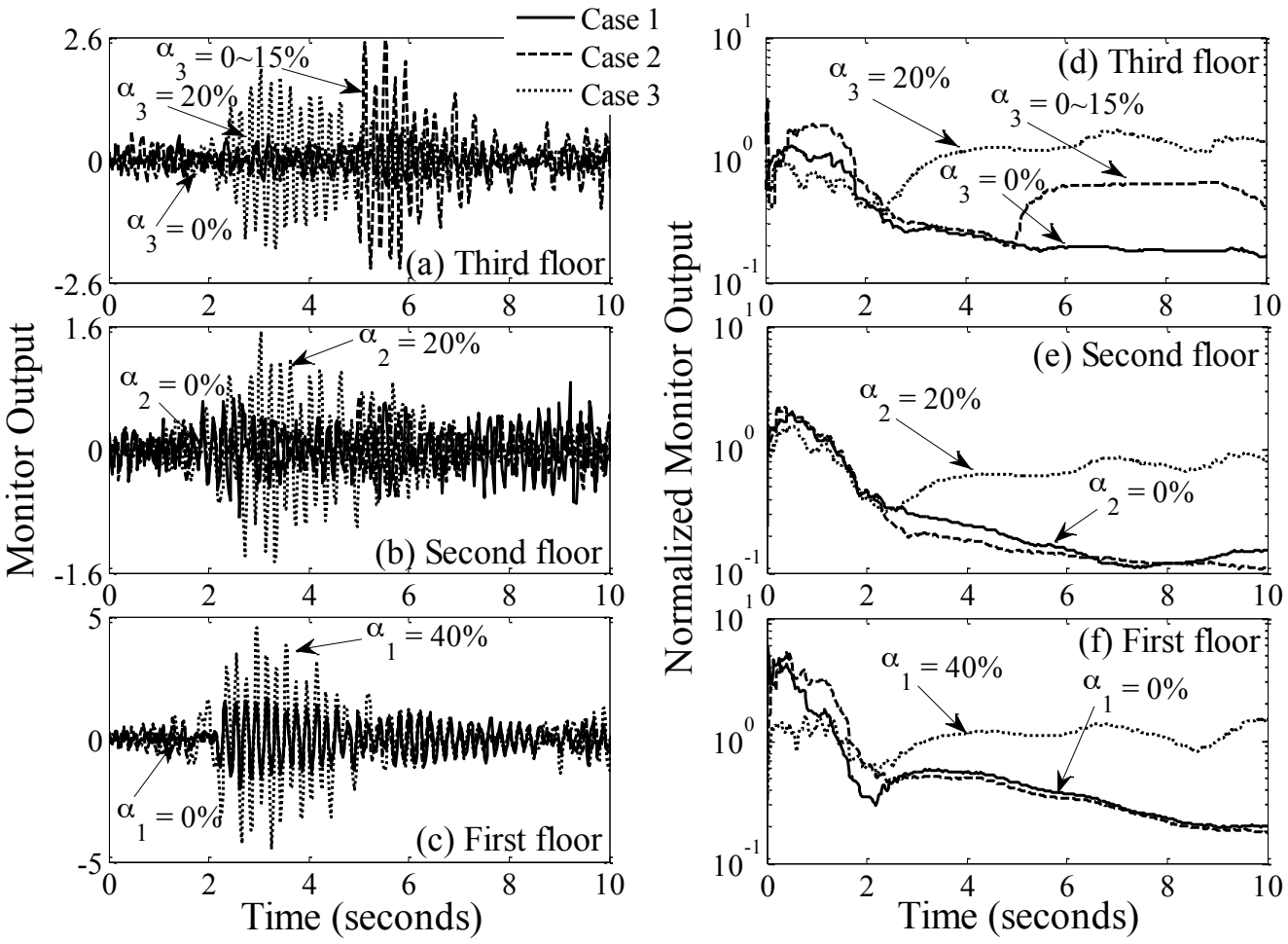


**Figure 2.** Damage identification for different scenarios of the three-story numerical model: (a)-(c) are original monitor output for case 1-3; (d)-(f) are normalized monitor output for case 1-3, where in case 1: $\alpha_1 = \alpha_2 = \alpha_3 = 0$; case 2: $\alpha_1 = \alpha_2 = 0$, $\alpha_3 = 0$ at $t < 5\,\text{sec}$, $\alpha_3 = 15\%$ at $t \geq 5\,\text{sec}$; case 3: $\alpha_1 = 40\%$, $\alpha_2 = 20\%$, $\alpha_3 = 20\%$

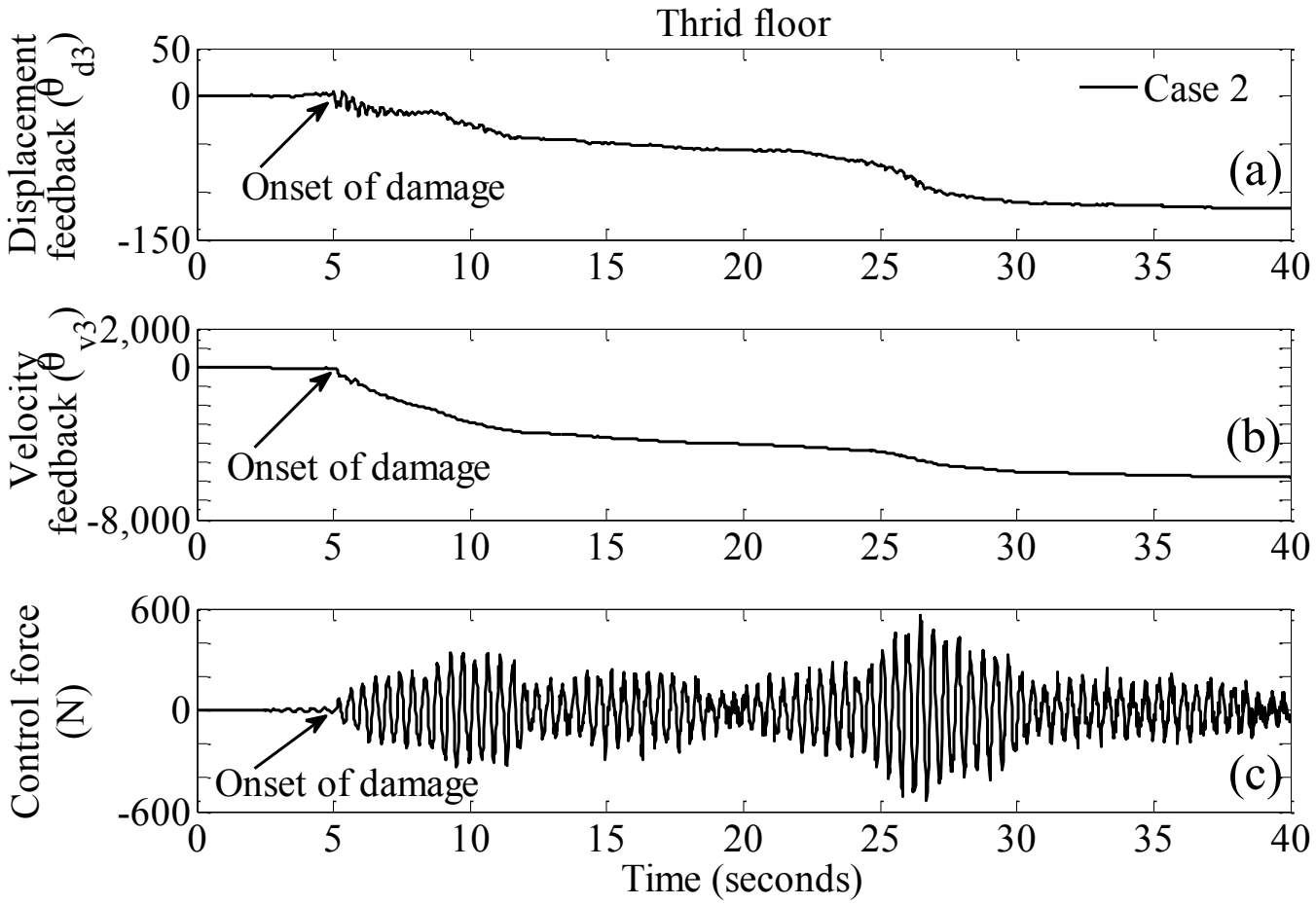


**Figure 3.** Time history of two time-varying adjustable parameters and the corresponding control forces on the third floor in case 2

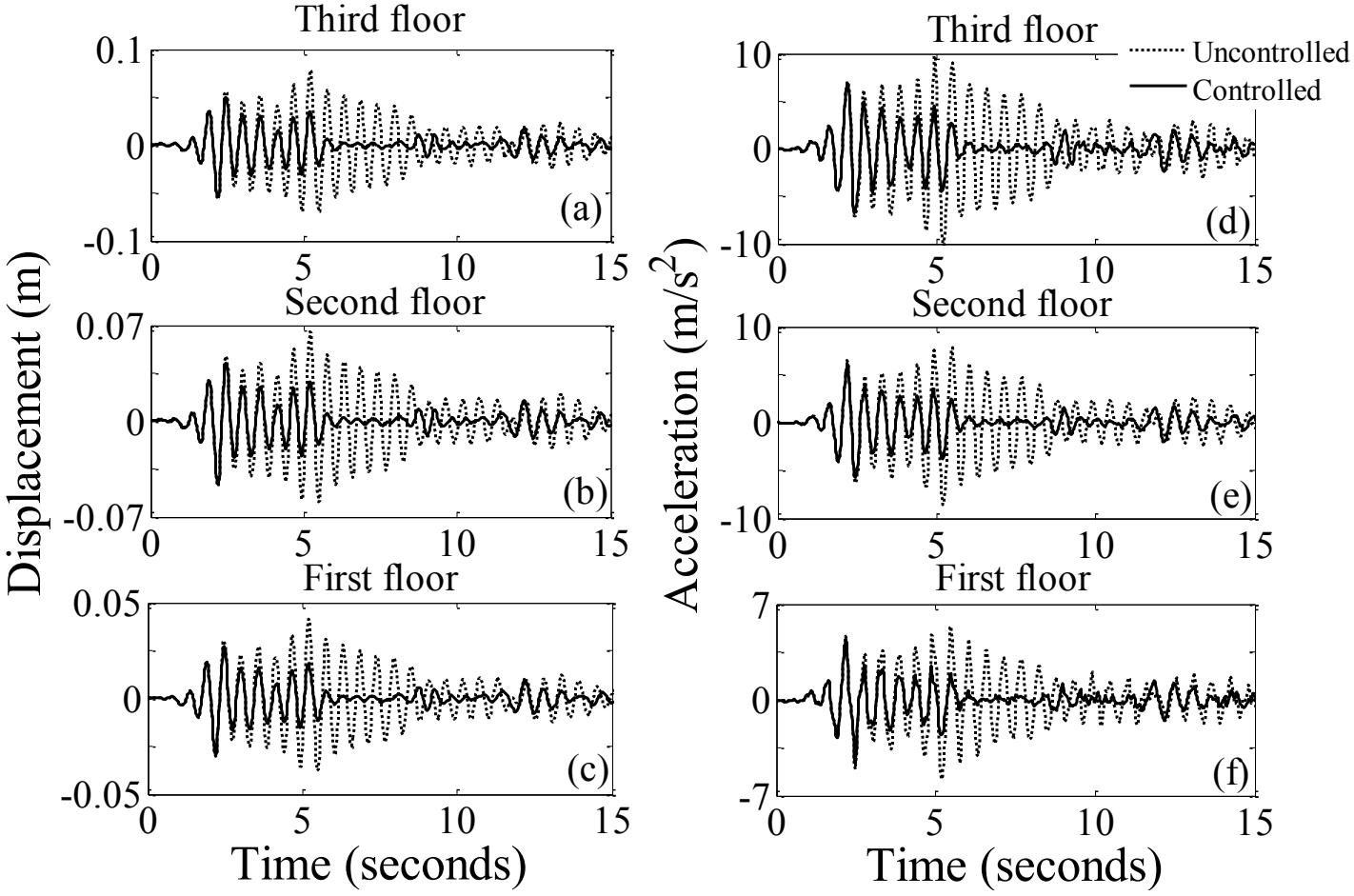


**Figure 4.** Comparison of response time histories of the three floors in case 3, with (a)-(c) for displacements, and (d)-(f) for accelerations on the three respective floors

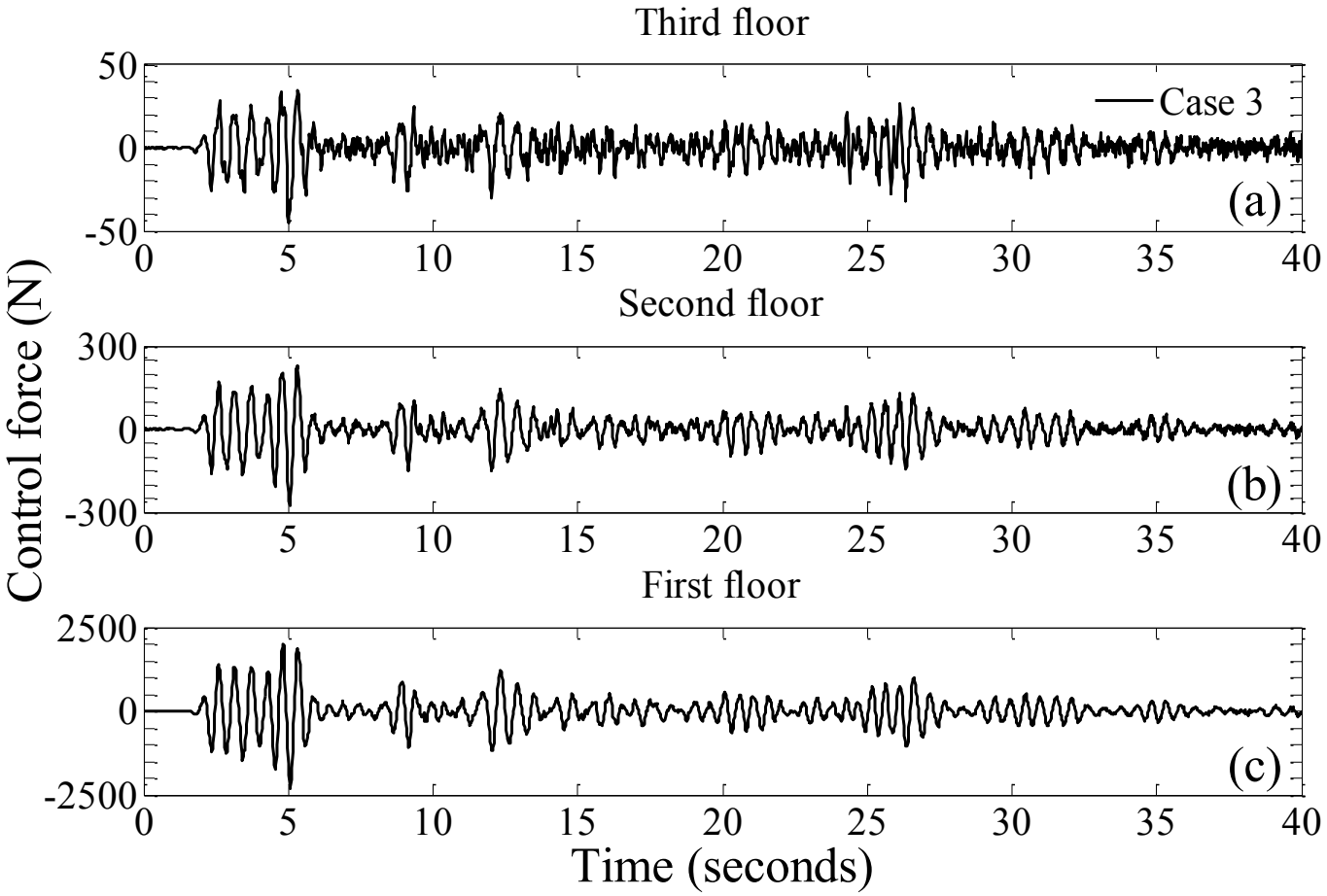


**Figure 5.** Time history of control forces on the three respective floors in case 3

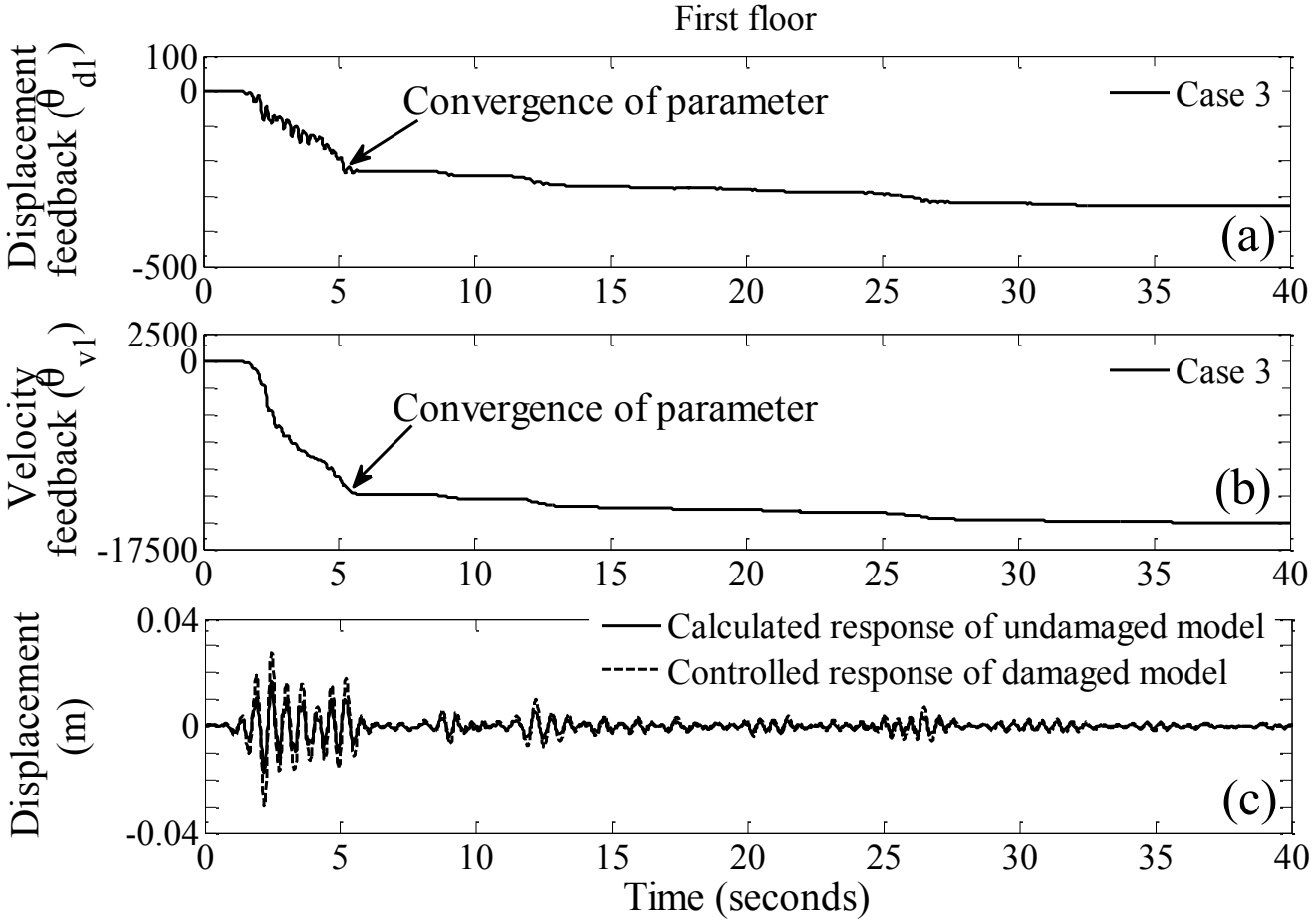


**Figure 6.** Shown in (a) and (b) are the time histories of two time-varying adjustable parameters, and shown in (c) are the calculated displacement responses of undamaged model and actual controlled displacement response of damaged model on the first floor in case 3

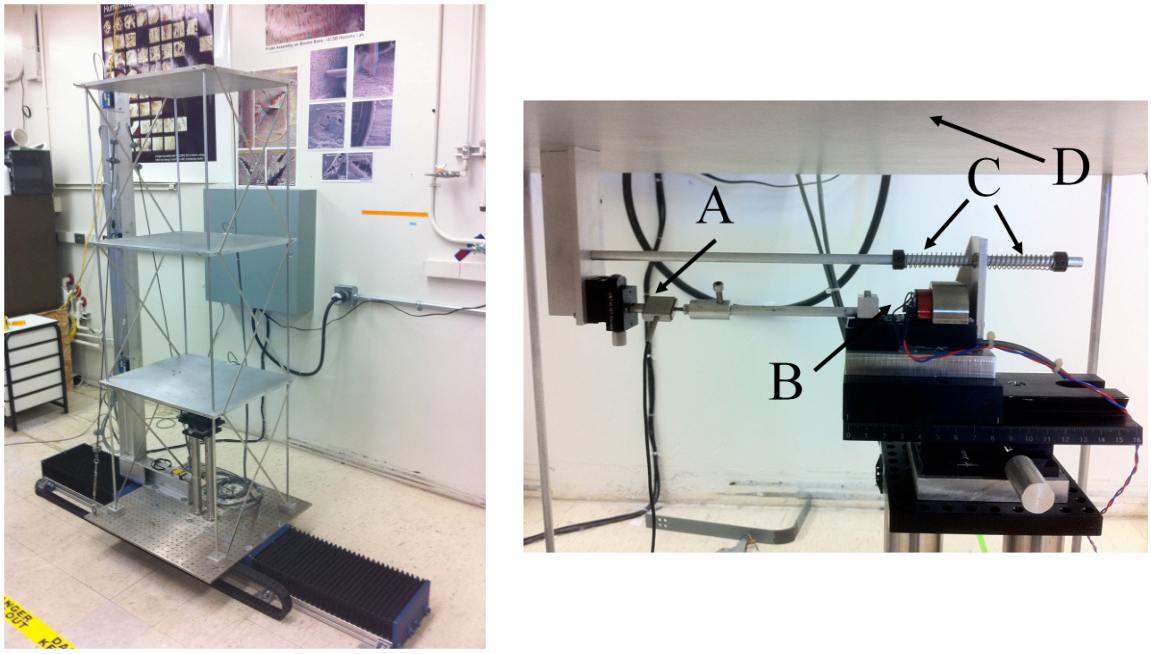


(a) (b)

**Figure 7.** (a) The experimental three-story aluminum frame structure; (b) The active actuator and stiffness change device installed to the first floor of the three-story aluminum structure. The components of this system comprise of: A-force transducer, B-active actuator, C-attached springs, and D-first floor plane;

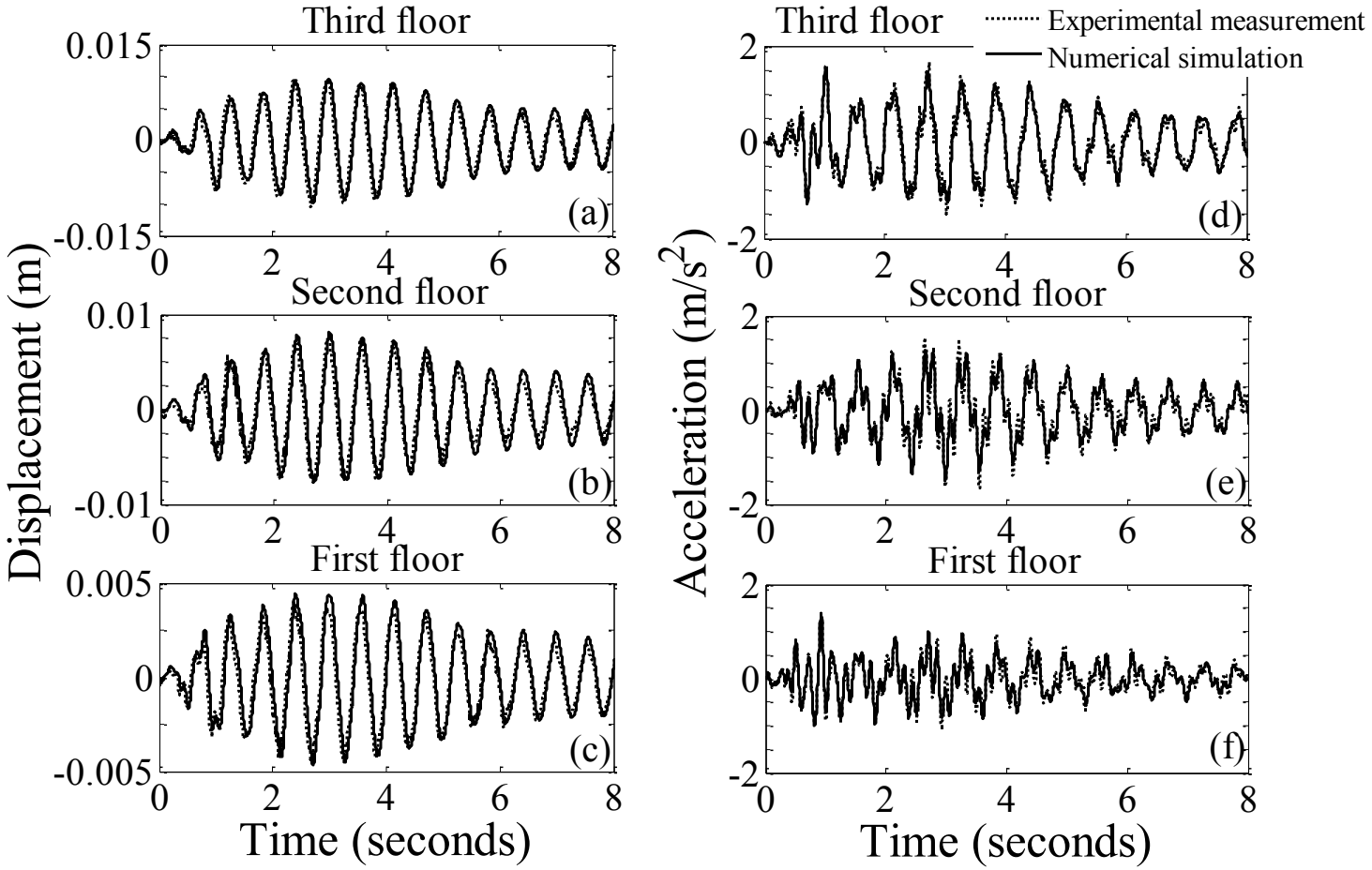


**Figure 8.** Comparison of the dynamic responses between the numerical simulation and experimental measurement of the three story aluminum model in scenario I (uncontrolled and $\alpha_1 = \alpha_2 = \alpha_3 = 0$) subjected to 1940 El Centro earthquake (N-S component), with (a)-(c) for displacements, and (d)-(f) for accelerations on the three respective floors

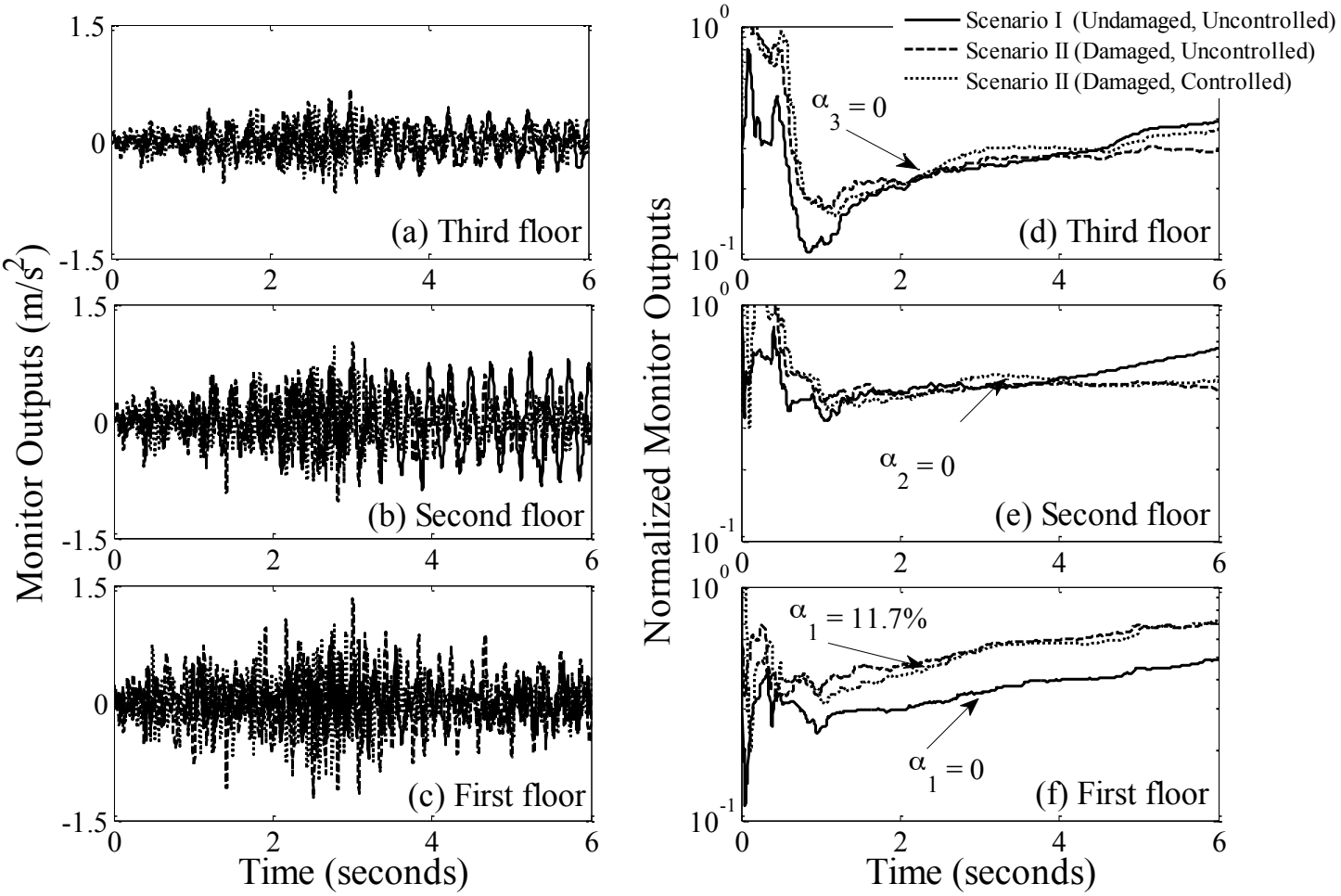


**Figure 9.** Original and normalized monitor output for three-story experimental structure in different stiffness scenarios: (a)-(c) are original monitor output, and (d)-(f) are normalized monitor output for scenario I ($\alpha_1 = \alpha_2 = \alpha_3 = 0$), II ($\alpha_1 = 11.7\%$, $\alpha_2 = \alpha_3 = 0$), respectively

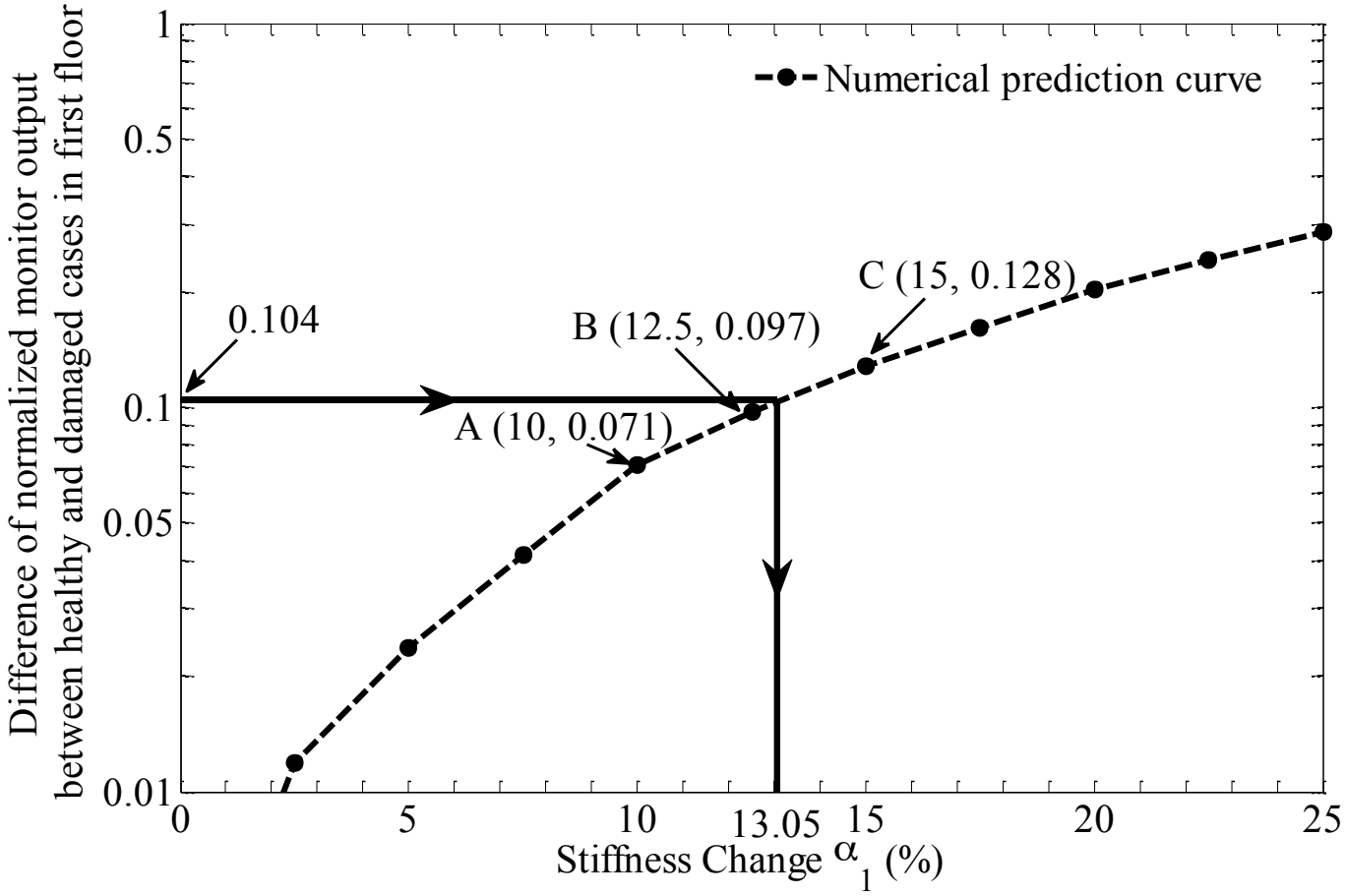


**Figure 10.** A numerical prediction curve for the first floor of the three-story structure using a linear interpolation prediction approach to predict the stiffness values in stiffness scenario II ( $\alpha_1 = 11.7\%,\ \alpha_2 = \alpha_3 = 0$ ) with control implementation

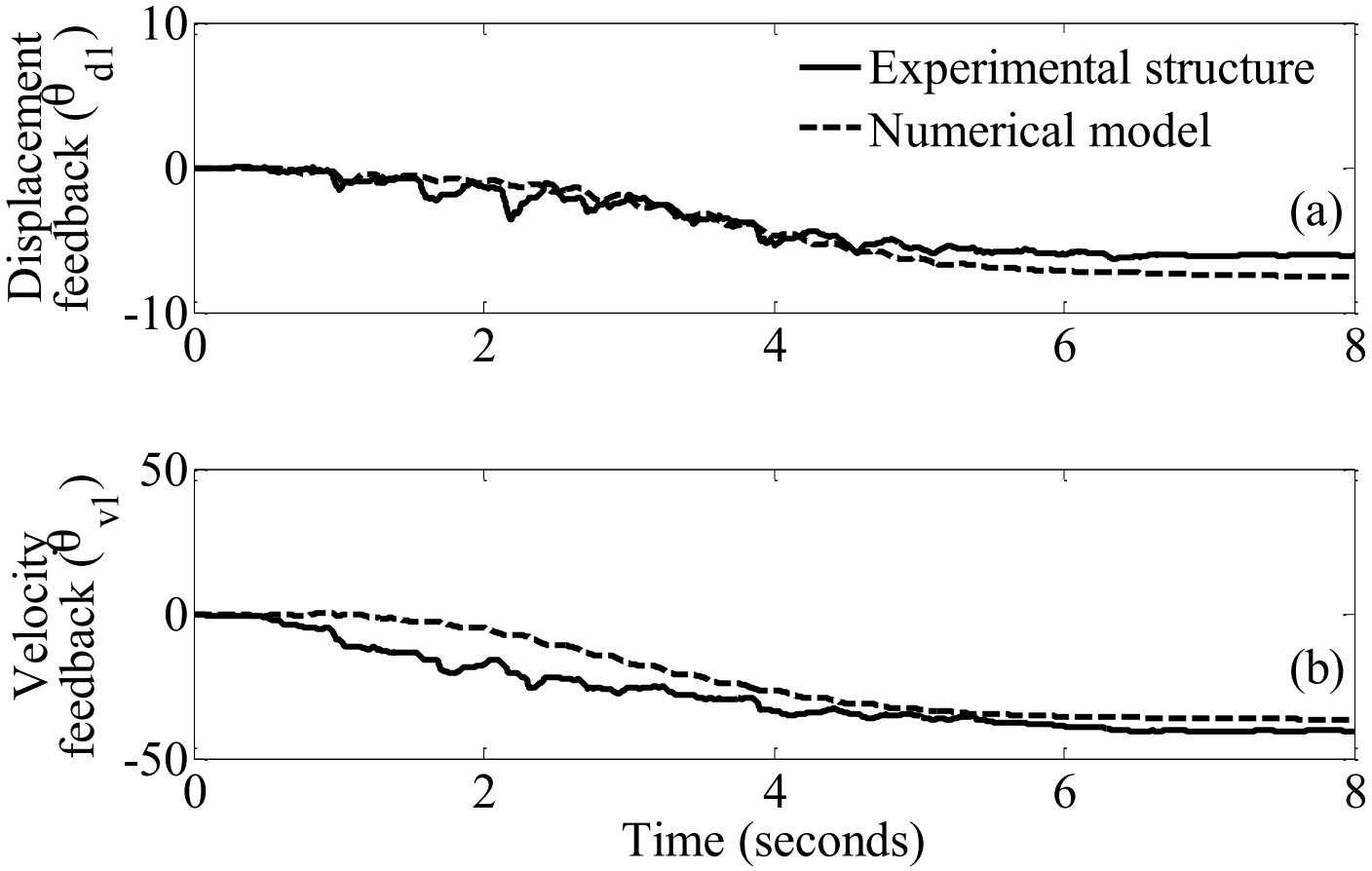


**Figure 11.** Comparison of updating and convergence of time-varying adjustable feedback parameters $\theta_d, \theta_v$ between experimental structure and numerical model

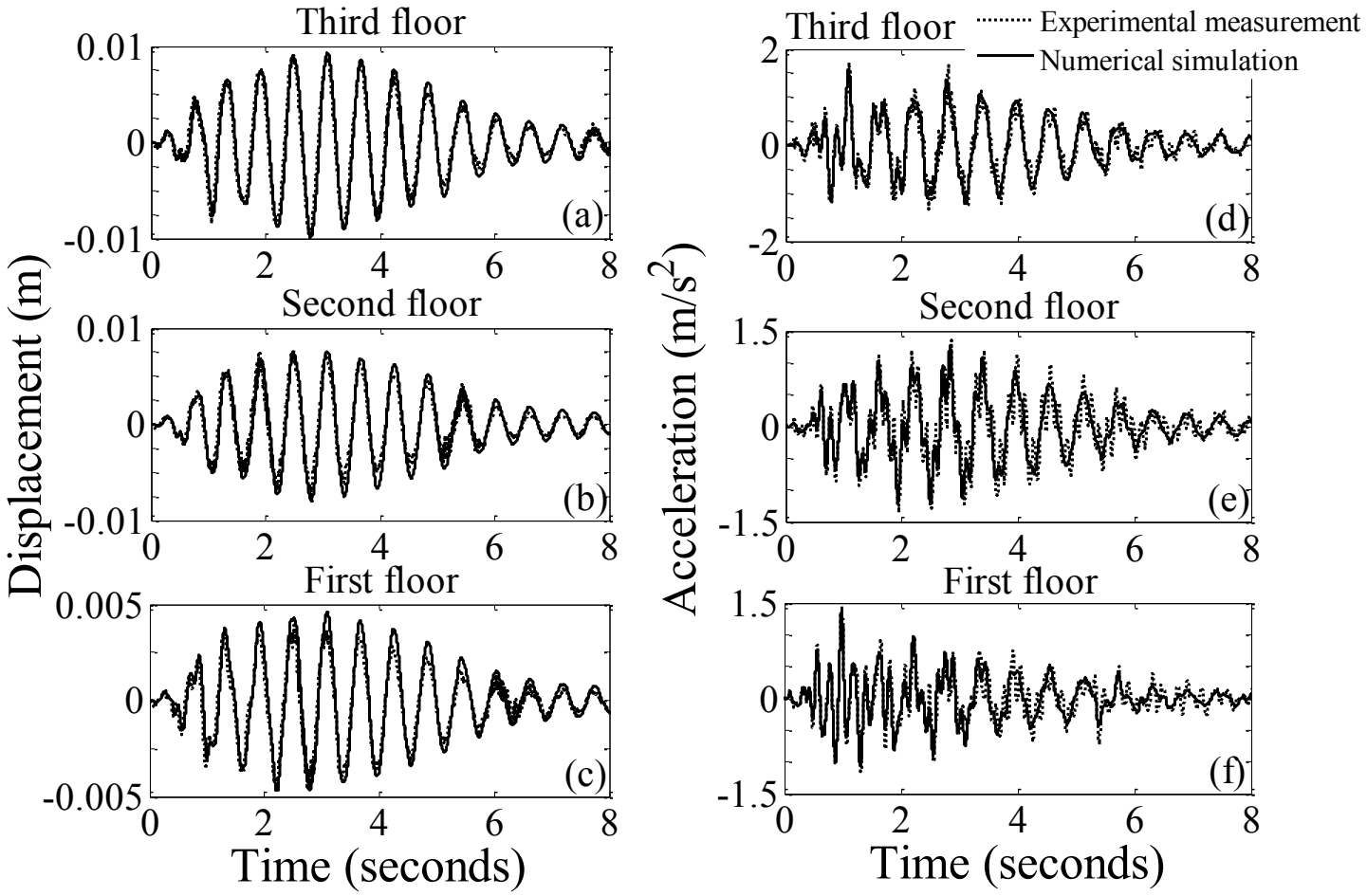


**Figure 12.** Comparison of the dynamic responses between numerical simulation and experimental measurement in stiffness scenario II ( $\alpha_1 = 11.7\%$ , $\alpha_2 = \alpha_3 = 0$ ) with adaptive control implementation under 1940 El Centro earthquake (N-S component), with (a)-(c) for displacements, and (d)-(f) for accelerations on the three respective floors

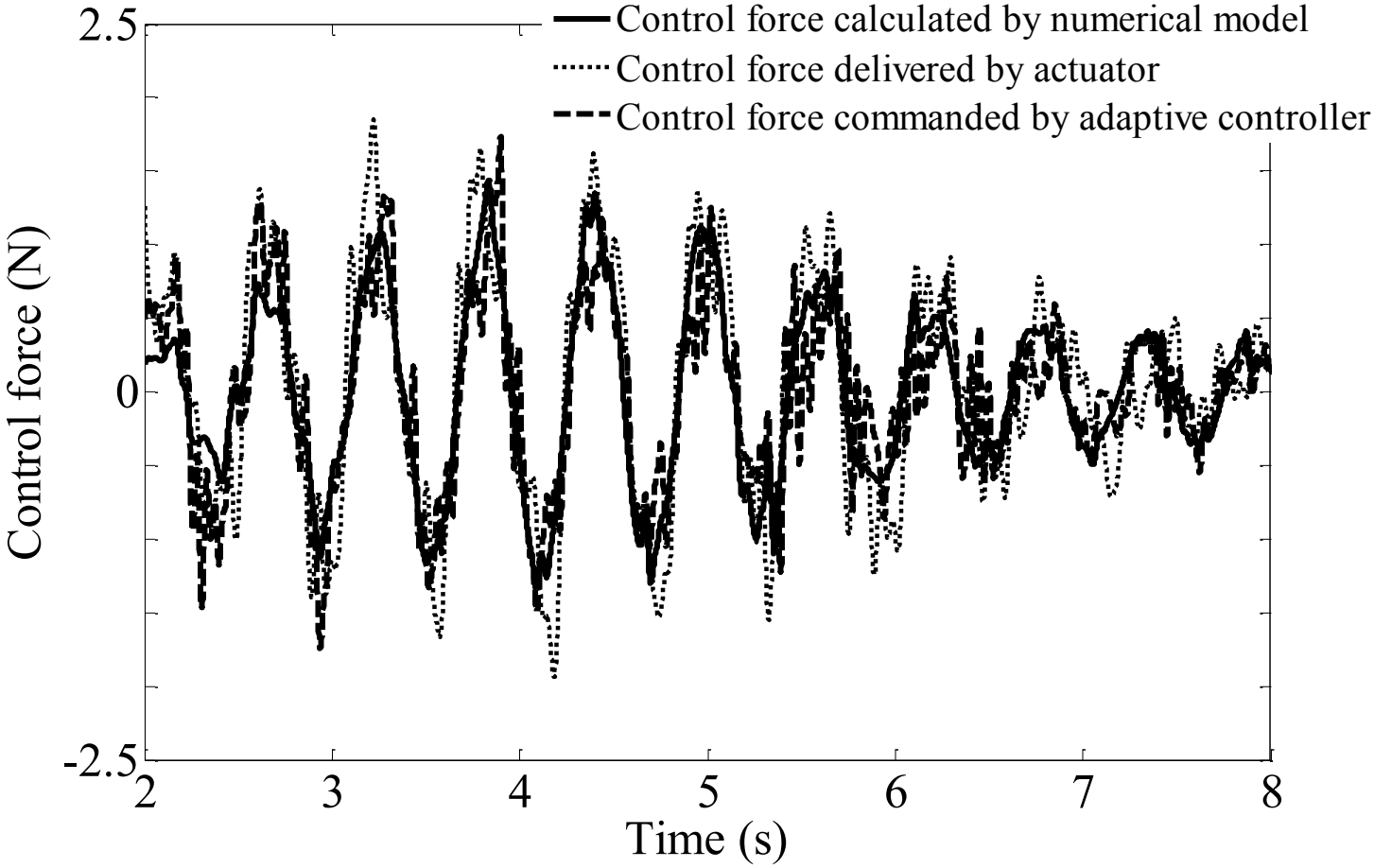


**Figure 13.** Comparison of the time history of the control force between experimental measurement and numerical simulation

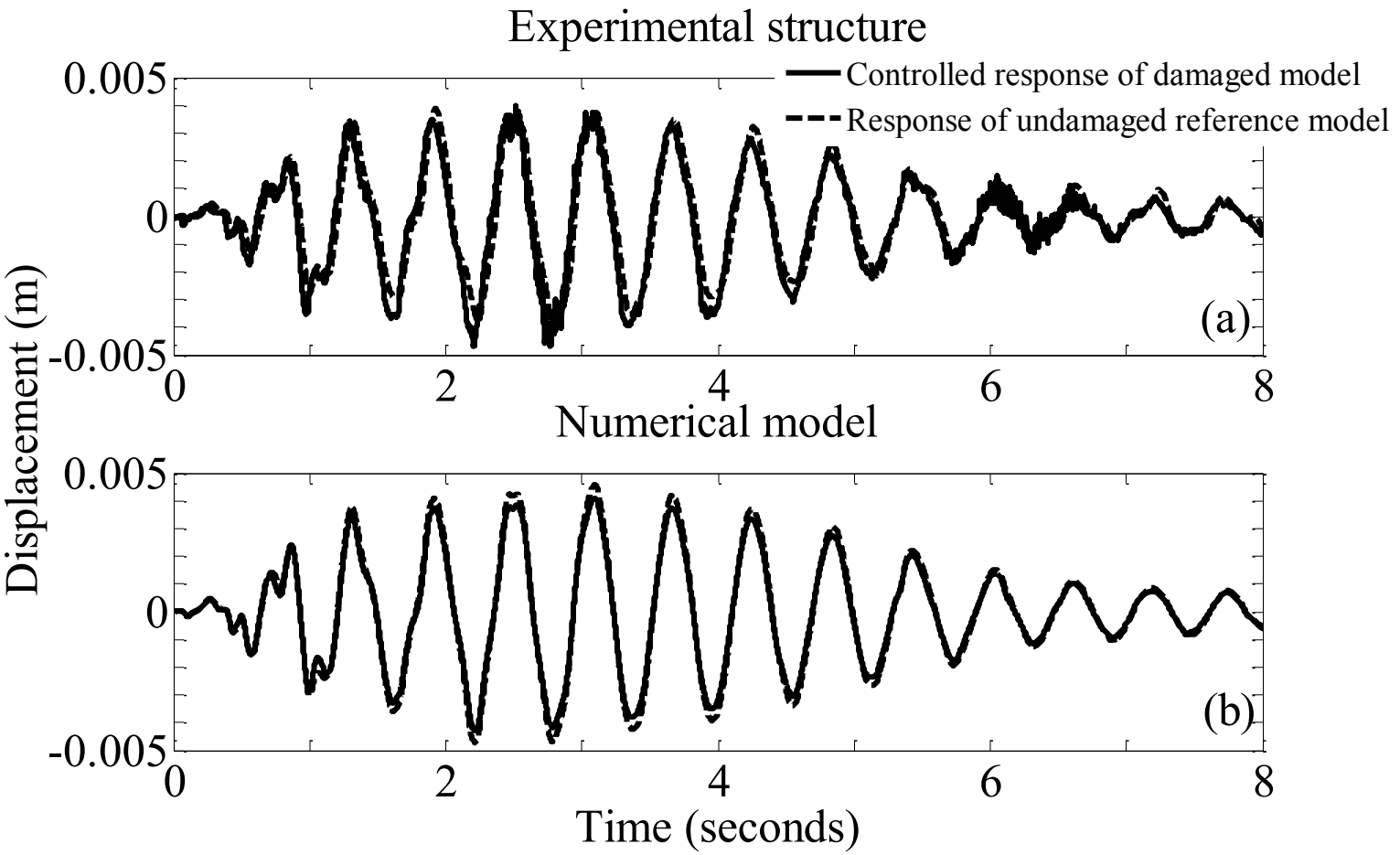


**Figure 14.** Experimental and numerical tracking performance of displacement on the first floor in stiffness scenario II ( $\alpha_1 = 11.7\%,\ \alpha_2 = \alpha_3 = 0$) with adaptive control

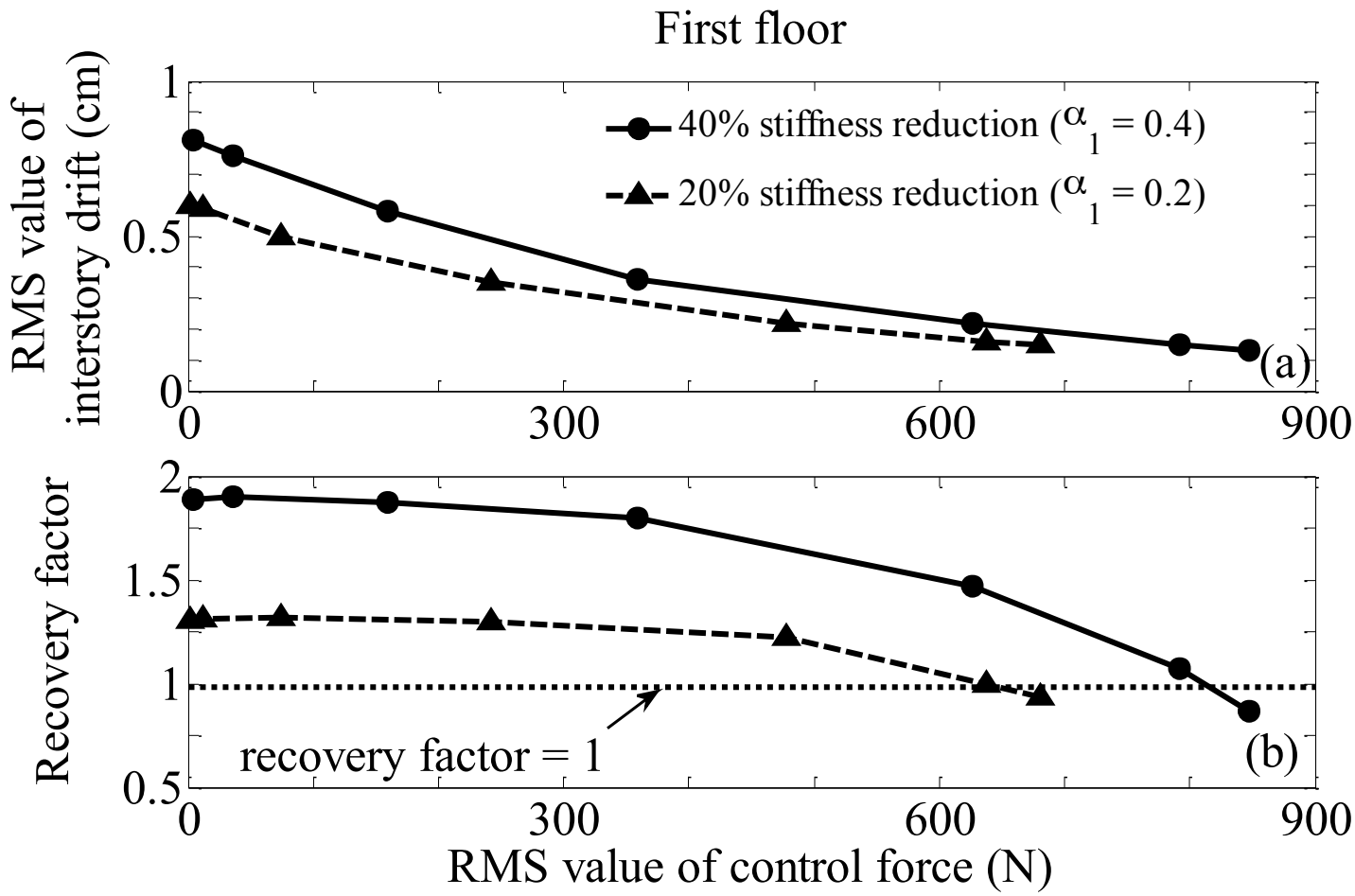


**Figure 15.** Parametric study: (a) is the relation between controlled interstory drifts and control forces in form of RMS value; (b) is the relation between recovery factors and RMS values of control force

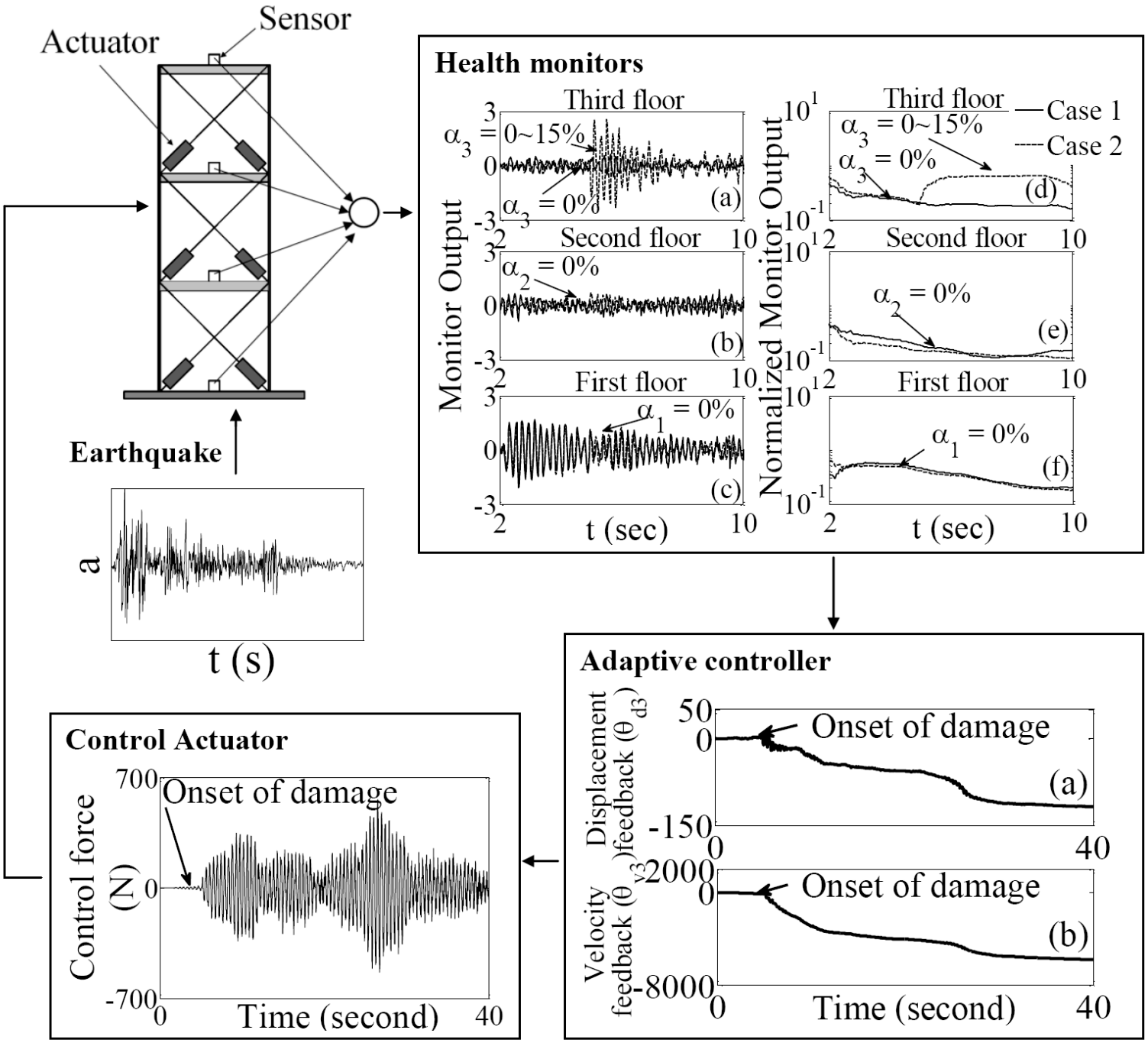


**Figure 16.** Illustration of the hybrid structural health monitoring and control system as given in Fig. 1 using the case 2 ( $\alpha_1 = \alpha_2 = 0$, $\alpha_3 = 0$ at $t < 5\,\text{sec}$, $\alpha_3 = 15\%$ at $t \geq 5\,\text{sec}$ ) in numerical simulation section shown in Figs 2 and 3